THE RESPONSE OF A MIXING LAYER FORMED BETWEEN PARALLEL STREAMS TO A CONCOMITANT EXCITATION AT TWO FREQUENCIES.

Ming de Zhou and I.Wygnanski*
Aerospace and Mechanical Engineering Department,
the University of Arizona, Tucson, Arizona.

August 1999

ABSTRACT[1]

Simultaneous excitation of a turbulent mixing layer by two frequencies, a fundamental and a subharmonic, was investigated experimentally. Plane perturbations were introduced to the flow at its origin by a small oscillating flap. The results describe two experiments that differ only in the amplitudes of the imposed perturbations and both are compared to the data acquired while the mixing layer was forced at a single frequency.

Conventional statistical quantities such as: mean velocity profiles, widths of the flow, turbulent intensities, spectra, phase-locked velocity and vorticity fields, as well as streak-lines were computed. The rate of spread of the flow under concomitant excitation at the two frequencies was much greater than under a single frequency although it remained dominated by two-dimensional eddies. The Reynolds stresses and turbulence production are associated with the deformation and orientation of the large coherent vortices. When the major axis of the coherent vortices starts leaning forward on the high velocity side of the flow, the production of turbulent energy changes sign (i.e. becomes negative) and it results in thinning the flow in the direction of streaming. It also indicates that energy is extracted from the turbulence to the mean motion. Resonance phenomena play an important role in the evolution of the flow. A vorticity budget showed that the change in mean vorticity was mainly caused by the nonlinear interaction between coherent vorticities. Nevertheless the locally dominant frequency scales the mean growth rate, the inclination and distortion of the mean velocity profiles as well as the phase-locked vorticity contours.

---

* Also the Faculty of Engineering, Tel Aviv University, Ramat-Aviv, 69978 Israel.

[1] The results presented are based on the data acquired at Tel Aviv University by I. Weisbrot in 1984. These results were never analyzed since the latter took a position in industry before completing his thesis work.

REPORT DOCUMENTATION PAGE

AFRL-SR-BL-TR-00-

0153

1. AGENCY USE ONLY (Leave blank)	2. REPORT DATE	3. REPORT TYPE AND DATES COVERED
		Final 10/01/97-09/30/99

4. TITLE AND SUBTITLE

The Response of a Mixing Layer Formed Between Parallel Streams in a Concomitant Excitation at Two Frequencies

5. FUNDING NUMBERS

F49620-96-1-0187

6. AUTHOR(S)

Israel Wygnanski, Professor

7. PERFORMING ORGANIZATION NAME(S) AND ADDRESS(ES)

Department of Aerospace and Mechanical Engineering
The College of Engineering and Mines
The University of Arizona
Tucson, AZ 85721

8. PERFORMING ORGANIZATION REPORT NUMBER

9. SPONSORING / MONITORING AGENCY NAME(S) AND ADDRESS(ES)

AFOSR/PKA
801 N. Randolpy Street
Arlington, VA 22203-1977

10. SPONSORING / MONITORING AGENCY REPORT NUMBER

11. SUPPLEMENTARY NOTES

12a. DISTRIBUTION / AVAILABILITY STATEMENT

Approved for Public Release - Distribution is Unlimited

12b. DISTRIBUTION CODE

13. ABSTRACT

Simultaneous excitation of a turbulent mixing layer by two frequencies, a fundamental and a subharmonic, was investigated experimentally. Plane perturbations were introduced to the flow at its origin by a small oscillating flap. The results describe two experiments that differ only in the amplitudes of the imposed perturbations and both are compared to the data acquired while the mixing layer was forced at a single frequency.

Conventional statistical quantities such as: mean velocity profiles, widths of the flow, turbulent intensities, spectra, phase-locked velocity and vorticity fields, as well as streak-lines were computed. The rate of spread of the flow under concomitant excitation at the two frequencies was much greater than under a single frequency although it remained dominated by two-dimensional eddies. The Reynolds stresses and turbulence production are associated with the deformation and orientation of the large coherent vortices. When the major axis of the coherent vortices starts leaning forward on the high velocity side of the flow, the production of turbulent energy changes sign (i.e. becomes negative) and it results in thinning the flow in the direction of streaming. It also indicates that energy is extracted from the turbulence to the mean motion. Resonance phenomena play an important role in the evolution of the flow. A vorticity budget showed that the change in mean vorticity was mainly caused by the nonlinear interaction between coherent vorticities. Nevertheless the locally dominant frequency scales the mean growth rate, the inclination and distortion of the mean velocity profiles as well as the phase-locked vorticity contours.

14. SUBJECT TERMS

15. NUMBER OF PAGES

43 + Attachment

16. PRICE CODE

17. SECURITY CLASSIFICATION OF REPORT	18. SECURITY CLASSIFICATION OF THIS PAGE	19. SECURITY CLASSIFICATION OF ABSTRACT	20. LIMITATION OF ABSTRACT
UNCLASSIFIED	UNCLASSIFIED	UNCLASSIFIED	UNLIMITED

INTRODUCTION

The turbulent mixing layer serves as a prototypical free shear flow and it was therefore most frequently investigated. At first, the research was limited to a statistical description of the flow, but since 1970s, it focused on conditional statistics and on coherent structures (Wygnanski & Fiedler 1970, Brown & Roshko 1974, Winant & Browand 1974; Browand & Weidman 1976; Wygnanski et al. 1979; Hussain 1983 etc.). When it was realized that the coherent structures play a central role in the evolution of the mixing layer, artificial excitation was soon to follow (Oster et al. 1978; Oster & Wygnanski 1982; Ho & Huang 1982; Gaster et al. 1985; Fiedler & Mensing 1985). Fiedler et al. (1981), Oster et al (1982) and Monkewitz and Huerre (1982) used the parallel, linear stability analysis to predict the most amplified frequencies and the amplification rates of the large eddies in the externally excited turbulent mixing layer while others used modeling and numerical simulation to obtain similar results (Patnaik et al. 1976; Acton 1976; Ashurst 1979; Riley & Metcalfe 1980, Corcos & Sherman 1984, Inoue & Leonard 1987; Inoue 1989). Gaster et al (1985) have demonstrated the significance of the flow divergence on the evolution of the large coherent structures and the ability of the stability approach to predict it in great detail. All of these articles revealed that selective, periodic disturbances strongly influence the coherent structures in the flow and its development in the direction of streaming. Weakly nonlinear analysis (Kelly 1967, Monkewitz 1982) suggested that a mixing layer might be more sensitive to an external excitation by two frequencies, a fundamental and its subharmonic, because the amplification of the latter could be affected by the presence of the former. Experiments (Zhang et al. 1984, Wygnanski and Petersen 1987) and numerical simulations (Inoue 1989; 1992) revealed that a concomitant periodic forcing at these two frequencies affected the evolution of coherent structures and increased the spreading rate of the mean flow beyond the values attained by single frequency excitation.

The task of enhancing the entrainment ability of the mixing layer was reinforced recently by the quest to delay flow separation through controlled periodic perturbations. The ideas were first articulated by Katz et al. (1989) and by Neuburger et al. (1988) who showed that detached flow forms a mixing layer that separates between a "dead-water" region adjacent to the surface and a constant velocity stream further away from it. The mean streamlines in the "free stream" above such a mixing layer are seldom curved and they do not diverge in the direction of streaming. Consequently, one would like to generate a sufficient pressure difference across this mixing layer that will force it to bend toward the surface. The most obvious way to attain it is, by bringing the surface close enough to the mixing layer thus reducing the size of the reservoir of fluid available for entrainment by the low velocity side of the mixing layer. One may also achieve a similar result by enhancing the entrainment rate of the mixing layer from the limited reservoir of fluid bound by it and by the solid surface. A bubble whose existence is deduced from time-mean data in highly turbulent flow nearing separation represents a delicate balance between the adverse force slowing down the flow

and promoting its separation and the force normal to the mean streamlines that keeps the mixing layer attached. We are interested therefore in exploring the role of the twin frequency excitation in the promotion of flow reattachment or the delay of its separation.

Since the mixing layer is perhaps, the simplest turbulent shear flow occurring in nature, a better understanding of its features may improve our understanding of turbulence in general. For example: What is the role of large coherent structures in the production of turbulence, how does it relate to nonlinear wave interactions, how one assesses the inter relation between coherent structures and typical random quantities. The measurements carried out by Weisbrot provide some information to the above mentioned problems. For example, the various Reynolds stresses (both coherent and incoherent) have been carefully scrutinized in order to explain the dependence of the flow on coherent structures and on the various possible interactions among those structures.

The experiments were carried out in a facility described by Oster and Wygnanski (1982) and slightly modified by Weisbrot et al (1988). Three sets of data were acquired with the first one being referred to as the "single frequency " (***SF***) case. It represents a mixing layer formed between two parallel streams of different velocities 10 & 6m/s respectively. The flow was excited by a single "fundamental", initially unstable frequency of 44.5 Hz. Measurements were made across the flow starting at x=200mm from the splitter plate and terminating at x=1720mms at streamwise intervals of 20mm. The other two data sets were labeled as "two frequencies-strong" (***TFS***) and "two frequencies-weak" (***TFW***) because of a difference in the relative amplitude of the excitation. The velocity ratio between the two streams bounding the mixing layer, $R=(U_1-U_2)/(U_1+U_2)$, remained identical for all three experiments. The ***TFS*** and the ***TFW*** sets were forced at a fundamental frequency of 36Hz and its subharmonic of 18Hz simultaneously. The displacement amplitude of the oscillating flap was 3.8mm for the fundamental and 4mm for the subharmonic for the set labeled "two frequencies-strong"; the respective amplitudes for the weak excitation were 1mm and 0.46mm. Two components of velocity were measured instantaneously at 7 transverse locations by using a hot-wire rake containing 14 wires configured in 7 X-wire arrays. The rake was traversed across the flow until the velocity gradients and the turbulent intensity became vanishingly small. Two reference signals and all individual velocity components were digitized and stored.

The instantaneous velocity was decomposed into a time mean quantity, a phase locked fluctuation $\langle u \rangle$ and the random residue: $u=U+\langle u \rangle+u_r$. We are fully aware that the coherent portion of the motion may be smeared-out by phase jitter and therefore poorly represented by a phase locked and ensemble averaged quantity (Zhou et al. 1996). However, the phase jitter of the dominant structures in the present flows, was quite small. Thus the coherent energy and Reynolds stresses obtained from simple, phase-locked data and from the more complex, temporal pattern matching (Zhou et al 1996), were not materially different. Consequently only the conventional phase-locked and ensemble averaged results are presented. Various aspects of the coherent motions, including phase-locked turbulent energy and Reynolds stress, phase and amplitude distributions of the individual components of the disturbances, coherent vorticity contours and coherent

streak lines were calculated from the data. Based on these results, the relation between coherent motions and the growth of the layer was observed.

RESULTS AND DISCUSSION

1. The Mean Flow

Streamwise distributions of the momentum thickness[2]

$$\theta = \int_{-\infty}^{\infty} \frac{U - U_1}{U_2 - U_1}\left[1 - \frac{U - U_1}{U_2 - U_1}\right] dy$$

are shown in Fig.1.1 for the three different excitations considered. It can be seen that the rate of spread of these flows differs from case to case and also from region to region in a single case. When the mixing layer was excited by a single frequency (labeled ***SF***) the momentum thickness increased up to x=560mm from the trailing edge of the splitter plate (region ***1*** in the parlance of Oster et al, 1982). It then ebbed and decreased with increasing streamwise direction up to x=840mm (region ***2***). Thereafter it resumed its growth but at a much smaller rate. The data set labeled "two frequencies-weak" (or ***TFW***) shows a similar trend, however, its growth rate in region ***1*** is slightly smaller than for the "single frequency" set. Its rate of spread in region ***3***, however is almost identical to that in region ***1*** and considerably larger than the corresponding region for the single frequency excitation. Furthermore, the onset of region ***2*** starts further downstream in this flow (x=950mm.), nevertheless the final width of the flow at x=1580mm was 25% larger than the flow that was excited by a single frequency. The momentum thickness resulting from stronger excitation (the "two frequency-strong" case that is also labeled as ***TFS***) increases monotonically in the direction of streaming, nevertheless the initial rate of growth for x<500mm is much larger than the final one. The final rate of growth in this case is almost the same as the final rate of growth in the ***TFW*** experiment. **It is clear that strong, concomitant excitation at two frequencies can double the final width of the flow relative to the single frequency excitation.**

The different rates of spread plotted in Figure 1.1 show the dependence of the mean flow on the excitation levels at the respective frequencies. The spreading rate is tied, in turn to the turbulence production and therefore the latter is also plotted in Figure 1.1 and will be discussed later.

In order to pinpoint the regions most affected by the external excitation the borders and the center of the mixing layer were arbitrarily defined by three numbers expressing the location on the mean velocity profile:

$Y_{0.1}$ represents the y location where the local mean velocity $(U-U_1)/(U_2-U_1)=0.1$, and represents the border of the mixing layer with the low-speed stream,

$Y_{0.95}$ defines the y location at which $(U-U_1)/(U_2-U_1)=0.95$ and thus represents the border of the mixing layer with the high-speed stream,

$Y_{0.5}$ describes the locus of points at which $(U-U_1)/(U_2-U_1)=0.5$ and it represents the center of the flow.

---

[2] This is an integral length scale whose integrand vanishes at both integration limits.

The streamwise distributions of $Y_{0.1}$, $Y_{0.5}$ and $Y_{0.95}$ are shown in Fig.1.2. The lateral rate of spread of $Y_{0.95}$ was initially (for x<330mm) quite rapid for the single frequency (***SF***) excitation and for the strongly excited flow at two frequencies (***TFS***) but it was almost nil for the ***TFW*** excitation. For 330<x<550mm the lateral rate of spread of $Y_{0.95}$ increased for the ***TFW*** excitation while it decreased for the other two cases. For 550<x<1340mm $Y_{0.95}$ stopped its lateral rate of spread in the ***TFW*** and ***SF*** excited flows but it increased its rate of spread for the ***TFS*** flow. While $Y_{0.5}$ was identical for the ***TFW*** and ***SF*** excited flows through the entire range of streamwise distances considered, it was displaced laterally toward the low-speed stream for the ***TFS*** excitation at x>550mm. The lateral divergence between $Y_{0.95}$ and $Y_{0.5}$ that occurred at x>550mm for the ***TFS*** test was largely responsible for the final width of this flow at the end of the measurement domain. In contrast, the ***SF*** excitation resulted in the convergence between $Y_{0.1}$ and $Y_{0.5}$ at 550<x<840mm that reduced the width of the flow in this range (labeled as region ***2*** in Fig. 1.1). $Y_{0.1}$ maintained its lateral rate of spread for the ***TFW*** flow up to x=950mm and was responsible for the increased width of the mixing layer relative to the ***SF*** excitation. $Y_{0.1}$ resumed its lateral growth for this case only beyond x>1400mms, while in the interim (between 950 <x< 1400mm) it remained constant or even decreased slightly (Fig. 1.2). Consequently, while for ***TFW*** and ***SF*** excitation most of the spreading rate (and presumably mixing) occurs on the low velocity side of the flow, it switches sides in the ***TFS*** case. This observation deserves special attention as it may lead to improved mixing through the use of active flow control. One may also note that $Y_{0.1}$ undulates for the ***TFS*** case up to X≈600mm beyond which it spreads laterally in a linear fashion as it does in an unexcited mixing layer.

Normalized mean velocity profiles, $(U-U_1)/(U_2-U_1)$, corresponding to the three types of excitation are shown in Figs.1.3a-c. The ordinate in these figures is $(Y-Y_{0.5})/\theta$ and it is consistent with the definition of the center of the mixing layer. The velocity profiles in each region are self-similar but the similarity does not always hold throughout the domain of measurement (i.e. between regions). For ***SF*** forcing the slope of the velocity profile, dU/dY on the low-speed side of region ***1*** (dashed line)is larger than in region ***3*** (see symbols in Fig. 1.3a) while the opposite effect is seen on the high speed side. For ***TFW*** forcing there is almost a perfect self-similarity between regions ***1*** and ***3*** (Fig. 1.3b). In the case of ***TFS*** forcing at X>1000mm region (it is impossible to discuss this flow in terms of distinct three regions), there is a strong kink in the mean velocity profile that on the high-speed side and moves toward the center with increasing x (Fig. 1.3c). This deformation is closely related to the type of coherent motion dominating the flow (e.g. the frequency) in a given region, as it will be discussed later.

2. Reynolds stress and turbulent intensities.

The lateral distributions of Reynolds stress and two components of the turbulent intensity are shown in Fig.2.1-2.3 for the three flows considered. The first and last streamwise locations chosen correspond to regions ***1*** & ***3*** while the intermediate locations represent data taken in region ***2*** and its boundaries (i.e. transition regions between ***1-2*** and ***2-3***).

The Reynolds stresses are positive in regions *1* and *3* for ***SF*** and ***TFW*** (Fig. 2.1a & b) where the momentum thickness also increases (see Fig. 1.1). However, the sign of the Reynolds stress changes in region *2* and it is associated with a decrease of the momentum thickness in the direction of streaming. Typically, close to the end of region *1* of the ***SF*** case (i.e. for X≅540mm in Fig. 2.1a), the shear stress on the high-speed side of the mixing layer becomes gradually negative. At X=560mm, $d\theta/dX=0$ and the integral of the shear stress across the layer vanishes as well. Around X=800mm the Reynolds stress tends to become positive again and with it $d\theta/dX>0$. This location marks the transition to region *3* in Figure 1.1. One may observe that the maximum negative value of u'v' occurs in the center of the mixing layer in the ***SF*** case (Fig. 2.1a).

The results for the ***TFW*** excitation are similar to the ***SF*** flow, in particular the correlation between the integral of the Reynolds stress across the flow and the location corresponding to $d\theta/dX=0$. In region *2* (e.g. at X=1080mm), the shear stresses are negative across the layer. At X>1120mm, transition from region *2* to *3* occurs and the Reynolds stress becomes positive again (Fig. 2.1b). There are, however, interesting differences between the ***TFW*** and the ***SF*** cases during the transition from region *1* to *2*. In the ***TFW*** flow, the negative shear stress appears first on the low speed side and remains there throughout region *2* and the transition region between *2* and *3*. For the ***SF*** flow the negative shear stress appears first in the center, above (on the high speed side) the region of positive Reynolds stress. The transition from region *2* to *3* is associated with the generation of a new zone of positive Reynolds stress on the high velocity side of the flow. This region diffuses toward the low-speed side of the mixing layer with increasing X. Thus, whenever the Reynolds stress distribution has an "S" shape in the ***TFW*** case, the zone of positive stress is always on the high speed side (see the lateral stress distributions at X=1040 & 1120mm in Fig. 2.1b) while it switches from side to side in the ***SF*** experiment. In the ***TFS*** experiment $d\theta/dX>0$ everywhere and thus the integral of the shear stress never changes its sign. Out of the five locations plotted in Fig. 2.1c the first two are in a region of locally decaying Reynolds stress while the last three in a region of local amplification. It will be seen later that the abrupt increase in Reynolds stress for the last three locations is related to a corresponding change in the form of the coherent structures.

The corresponding distributions of the u' and v' are plotted in Figs.2.2 and 2.3. For the ***SF*** excitation the distribution of the u' at a given X contains two maxima separated by a saddle point in the center (see Fig. 2.2a at X=540 & X>800mm) while the v' distribution contains a single maximum at the center of the flow (Fig. 2.3a). Such intensity distributions are indicative of a single row of traveling vortices. A similar observation can be made for the ***TFW*** excitation around X≈980mm. On the other hand, for the ***TFW*** flow at X>1400 and for the ***TFS*** flow at X≈660 the u' distribution becomes extremely peaky while the v' distribution becomes broad and eventually develops two maxima with a saddle point in between. Further downstream the u' distribution develops three maxima, while the v' distributions get two (Figures 2.2c & 2.3c). These distributions suggest that a vortex pairing takes place in which some of the vortices that were originally in line got displaced laterally. When the initial displacement is comparable to a typical radius of a

vortex the u' component gets a strong peak in the center but as the displacement increases this peak may split into three (Fig. 2.2c X=1060mm).

The integrated values of u'^2, v'^2 and u'v' across the layer are shown in fig.2.4. Most interesting is the correlation between the sign of the integrated Reynolds stress and $d\theta/dX$ (Fig. 1.1). Whenever $\int u'v'dY<0$ so is $d\theta/dX$. The local maxima and minima of θ match the zero crossings of $\int u'v'dY$ perfectly for the ***SF*** and ***TFW*** experiments. In a mixing layer, θ represents an integral length scale whose integrand vanishes on both sides of the flow, thus the relationship between u'v' and θ differs from the relationship we are accustomed to in a boundary layer. However, since dU/dY in mixing layer is always positive, the sign of shear stress determines the sign of the turbulence production. For this reason, the integrated turbulence production term $\int u'v'(dU/dY)dY$ is plotted in fig.1.1.

The integral value of $\int(u')^2\,dY$ is hardly amplified for the ***SF*** excitation before starting to decay slowly with increasing X. In the ***TFW*** case, the value of $\int(u')^2dY$ increased by a 50%, reached a plateau and then increased again when $\int(u'v')dY>0$. The value of $\int(v')^2dY$ in this case, attained an amplification of 440% just prior to the location at which $\int(u'v')dY$ became negative at X=950. In the ***TFS*** case the amplitude of $\int(v')^2dY$ increased in a stepwise manner, first by a factor of 2, then to 3 before resuming continuous growth and attaining a factor of 5.5 at the end of the measurement domain.

There is an exchange of energy between the two components of turbulence intensity that is most obvious for the ***SF*** excitation. For example: a saddle point in the $\int(u')^2\,dY$ occurring at X=550mm, corresponds to a maximum in the $\int(v')^2\,dY$. The relationship between the two fluctuating components in the ***TFW*** and ***TFS*** experiments is more subtle but it exists non the less. These relationships imply that significant energy is contained in large two dimensional eddies as already observed by Gaster, Kit and Wygnanski (1985). These relationships will be better understood when the phase-locked and ensemble-averaged data of a given scale will be processed

3. Mean Momentum Balance.

In order to check the two-dimensionality of the flow and to some extent the reliability of the measurements, the Reynolds stress distributions were calculated from the two dimensional momentum equation:

$$-\frac{\overline{uv}}{(U_2-U_1)^2}=\frac{1}{(U_2-U_1)^2}\int_{-\infty}^{y}[\overline{U}\frac{\partial\overline{U}}{\partial x}+\overline{V}\frac{\partial\overline{U}}{\partial y}+\frac{\partial}{\partial x}(u'^2-v'^2)]dy$$

while the continuity equation yields:

$$\overline{V}=-\int_{-\infty}^{y}\frac{\partial\overline{U}}{\partial x}dy+V_{-\infty}$$

where:

$$\frac{V_{-\infty}}{U_2 - U_1} = \frac{1}{(U_2 - U_1)^2} \int_{-\infty}^{\infty} \frac{d}{dx}[(\overline{U} - U_1)\overline{U} + u'^2 - v'^2]dy$$

The integration was initiated on the high-speed side from a Y location corresponding to a vanishing velocity gradient. The normal mean velocity component V, used in the momentum balance was not measured but rather calculated from the continuity equation because measurements of V with hot wires are notoriously inaccurate in turbulent shear flows. The values of V at infinity were determined by iterative procedure requiring that the Reynolds stress on the opposite side of integration domain will vanish. This criterion was independent of the side at which the integration was initiated. The entrainment field results in a pressure gradient that is neglected by the boundary layer approximation. Dropping the pressure gradient at the integration boundaries resulted in an error that was most apparent at the boundaries. Thus a free stream pressure gradient was imposed at the boundaries of the integration. Since the streamwise velocity gradients on the high-speed boundary of the flow are not the same as on the low speed side, the local pressure gradient was calculated from linearly interpolated values across the layer.

The results of these calculations are marked by solid curves in fig.2.1. There is good agreement between calculations and measurements for the ***TFW*** and ***TFS*** cases throughout the measurement domain and in region ***1*** of the ***SF*** experiment where the calculated positive Reynolds stress matches the measured data very well. In the transition regions marking the boundaries between ***1*** and ***2*** or ***2*** and ***3*** of ***SF*** , the calculated shear stresses match all the important features of the experiment, including the appearance of the negative shear stress starting on the high-speed side of the flow. At x=560mm, where $d\theta/dX=0$, the integral of the calculated shear stress across the layer also vanished. In region ***3*** however, there is a considerable discrepancy between the calculated Reynolds stress and the data measured for the ***SF*** experiment. This raises some questions about the two-dimensionality of the flow near the end of the measurement domain where the coherent eddies become weak.

4.Spectra.

The existence of coherent structures in turbulent flows can be detected through spectral analysis. Even in the absence of external excitation, a spectral peak appearing in the low frequency range can often be identified with a wavy disturbance that had undergone the largest possible amplification. These predominant frequencies may vary somewhat across the flow because of its divergence in the direction of streaming (Crighton & Gaster 1976). Spectral analysis can provide extensive information about energy transfers that take place in externally excited flows.

The power spectra of the v' fluctuations and the cross spectra of u'v' measured at various x locations close to center line of the layer are shown in Fig. 4.1 and 4.2. The power spectra of the u' fluctuations are not shown for the sake of brevity because, for a two-dimensional perturbation, the two distributions (u' & v') are related through continuity and are usually delayed in phase. Furthermore, the preferred locations to track

the u' fluctuations are at the edges of the shear layer and not its center (consider an array of co-rotating eddies located on a centerline of the mixing layer such as were observed by Oster et al 1978).

For the ***SF*** excitation the fundamental frequency dominates the entire flow (Fig. 4.1a) with a weak harmonic being present at the end of region ***1*** due to the relatively large amplitude of the fundamental. No subharmonic frequency was observed suggesting that "vortex pairing" is inhibited by the single frequency harmonic excitation. The cross-spectrum is also dominated by the excitation frequency even though it is an order of magnitude weaker than the power spectrum (Fig. 4.2a). The streamwise location at which the cross spectrum becomes negative (indicating the possible existence of a negative Reynolds stress) corresponds to the location at which v' attained its maximum amplitude. Consequently this is the location at which the mean flow became neutrally stable relative to the imposed disturbance.

Similar observation can be made for the ***TFW*** case, except that the peak in the power spectrum at the fundamental frequency is much higher and it occurs at a larger streamwise location (Fig 4.1b, see also Fig. 1.1b). Two additional observations can be made:

(i) The streamwise amplification of the subharmonic disturbance might not have attained its maximum at the end of the measurement domain because it was not initially amplified. It is interesting to note that the subharmonic excitation is hardly distinguishable from the background over 60% of the measurement domain (Fig.4.1b,4.2b). One may correlate this with the low amplification rate of the integrated intensity $\int v'^2 dy$ (Fig.2.4) observed at small distances for the ***TFW*** case.

(ii) On the other hand there is an early appearance of a wavy disturbance generated by the interaction of the two excited modes (i.e. 3/2 of the fundamental frequency). This suggests a transfer of energy from the imposed excitation to the interaction mode. Once again the location of the peak in the power spectrum corresponds to the onset of a negative cross-spectrum at f and 3/2f.

In the ***TFS*** case there is an early dominance of the 3/2f perturbation that overshadows the fundamental in spite of the fact that the latter frequency was externally forced upon the flow (Fig. 4.1c). The disturbance at the fundamental frequency, f, attained its first maximum level around X=340mm while the peak at the interaction frequency occurred soon thereafter (X=400mm) to be followed by the subharmonic disturbance (around X=600mm). The locations of these peaks in the spectrum correspond also to the locations at which undulations in $\int v'^2 dy$ occur. A second peak in the fundamental disturbance occurs further downstream (around X=650mm) where the cross spectrum at that particular frequency is negative. This suggests a strongly non-linear interaction among these three modes. The negative cross spectrum at the fundamental frequency corresponds to a local plateau in $\int u'v' dy$ shown in Fig.2.4. The dominance of the subarmonic (f/2) and the interaction (3/2f) modes in the power and cross spectra for the ***TFS*** excitation is another indication that a nonlinear mechanism is responsible for the energy exchanges that take place in this flow. In particular, downstream of the peak in

the *3f/2* power spectrum, there is no corresponding negative cross-spectrum region. It implies that the decay of the *3f/2* frequency is not due to the negative production or direct energy transfer back to the mean, but rather, due to transfer to other components through nonlinear interactions.

5. Phase-locked and Ensemble Averaged data.

One may assume that the coherent structures are represented by the phase locked and ensemble averaged velocity fluctuations. One may further decompose these coherent fluctuations in Fourier space to obtain the amplitudes of the leading spectral components in the flow. They correspond of course, to the two forcing frequencies and their sum, since these were also the leading spectral components observed in Fig. 4.1.

The spatial distribution of the prevailing disturbances (i.e. the fundamental, fo, the subharmonic, fo/2, and the leading interaction, 3fo/2) are shown in Figs. 5.1 to 5.3 at some selected streamwise locations. The data corresponding to the ***SF*** excitation for 200<X<560mm like the amplitude distribution of $\langle u \rangle_{fo}$, is well known (Gaster et al. 1985 and Weisbrot &Wygnanski 1988) because it represents a linearly amplifying mode. Around X≈550mm this mode ends its amplification cycle and starts to decay. The amplitude and phase distributions therefore, represent a typical array of eddies that span the entire width of the flow.

The initial evolution (for X<700mm) of the fundamental frequency in the ***TFW*** experiment is similar to ***SF*** forcing. However, toward the end of the measurement domain (i.e. for X> 1300mm.) the amplitude distributions of $\langle u \rangle_{fo}$ and $\langle v \rangle_{fo}$ indicate that the array of decaying vortices is being displaced laterally in an orderly staggered fashion. This is coupled with a typical, distribution of $\langle u \rangle_{fo/2}$ that is being amplified at X>1040mm. The distributions of fo and fo/2 amplitudes for the ***TFS*** excitation are similar to ***TFW*** except that they occur much closer to the origin of the flow. The stagger of the decaying vortices associated with the fundamental frequency occurs around X≈400mm and it evolves into two separate rows of vortices toward the end of the measurement domain (see the $\langle v \rangle_{fo}$ distribution in Fig. 5.3b at X=1340mm). The amplitude distributions of $\langle u \rangle_{fo/2}$ or $\langle v \rangle_{fo/2}$ measured at X>1000mm in the ***TFS*** case are not familiar from linear stability analysis. It is interesting to note that a very small amplitude of $\langle v \rangle_{fo/2}$ in the ***TFW*** case generates a substantial amplitude of the nonlinear interaction mode $\langle v \rangle_{3fo/2}$. This is particularly visible in the initial region (X<500mm in Fig.5.2b) where the fundamental frequency is being linearly amplified by extracting energy from the mean motion. At larger distances most of the energy is being absorbed by the subharmonic $\langle v \rangle_{fo/2}$. In the ***TFS*** case, where he initial amplitude of $\langle v \rangle_{fo/2}$ is equal to $\langle v \rangle_{fo}$, the interaction mode $\langle v \rangle_{3fo/2}$ is of comparable amplitude (see Fig. 5.3 for X<500mm). The relative intensity of the interaction mode, $\langle v \rangle_{3fo/2}$, in both flows decreased after the subharmonic became the dominant mode (see Figs. 5.2 & 5.3 for X>1300mm).

The various phase-locked quantities were integrated across the layer to obtain the streamwise variations of the coherent energy contained in the individual modes. The

results for $\int\langle u^2\rangle dy$, $\int\langle v^2\rangle dy$, $\int\langle uv\rangle dy$ and their leading coherent quantities are shown in Fig.5.4a-c respectively. The corresponding total turbulent intensities discussed previously are re-plotted here for comparison. The initial value of $\int\langle u^2\rangle dy$ for the ***SF*** excitation is approximately 70% of $\int u'^2 dy$ but it diminishes slowly to 25% at the end of the measurement domain. For the ***TFW*** case the initial level was only 55% yet it increased to 75% at large X, while for the ***TFS*** excitation this ratio remained at approximately constant level of 85% (see Fig. 5.4a). The ratio between $\int\langle v^2\rangle dy$ and $\int(v')^2 dy$ is usually larger than for the streamwise component of velocity and it exceeds 90% for the ***TFS*** excitation. The amplification ratios of the $\langle v\rangle_f$ component at the fundamental frequency are much larger than the amplification of the $\langle u\rangle_f$ component. For ***SF*** case, for example, $\int\langle u^2\rangle_f dy$ increased over its initial value by a mere 25% in region 1, it increased by 70% in region 1 of the ***TFW*** excitation but did not increase at all for ***TFS*** (Fig. 5.4a). The integrated normal component, $\int\langle v^2\rangle_f dy$, increased by 5 fold for ***SF,*** by 20 fold for ***TFW*** and only by a factor of 4 for ***TFS.*** The disparity in the amplification between the streamwise and normal components made the total, integrated turbulent energy behave like $\int\langle v^2\rangle_f dy$ thus the sum of the two components is not presented here. This is also the case for the subharmonic $\langle v\rangle_{f/2}$.which becomes dominant at the end of the measuring domain for the ***TFW*** excitation and dominates the flow beyond X>600mm for the ***TFS*** case.

Most of the coherent energy for the ***SF*** excitation is contained in the fundamental frequency with the subharmonic being insignificant everywhere (fig. 5.4). For the ***TFS*** excitation the initial forcing levels at fo & at fo/2 were comparable, however while the fundamental hardly amplified the subharmonic soared. It is worth mentioning that the interactive mode, 3fo/2, may play an important role in both ***TFW*** and ***TFS*** experiments. Its integrated energy attained the same level as the fundamental around X=350mm in the ***TFS*** case while exceeding the energy content of the subharmonic around X=500mm (fig. 5.4b) in the ***TFW*** experiment. In both ***TFW*** and ***TFS*** cases the subharmonic frequency got rapidly amplified after the fundamental started to decay suggesting possible energy exchange between fundamental and the subharmonic.

The contribution of the individual components to the Reynolds stress is shown in figure 5.4c. At small values of X, most of the coherent Reynolds stress is contained in the fundamental excitation frequency for the ***SF*** and the ***TFW*** flows but not in the ***TFS*** case that contains coherent stresses at fo, fo/2 and many higher harmonics. These are associated with the high forcing amplitudes. Wherever $\int\langle uv\rangle_f dy$ becomes negative during the ***SF*** experiment so does the integrated Reynolds stress $\int u'v' dy$. The latter changes sign (to become positive again) around X=840mm due to the contribution of random motion (Fig. 5.8c). In the ***TFW*** excitation the negative $\int\langle uv\rangle_f dy$ is offset by the positive $\int\langle uv\rangle_{f/2} dy$ making the overall Reynolds stress still negative but over a very short region. The positive contribution of the subharmonic $\int\langle uv\rangle_{f/2} dy$ in the ***TFS*** case overwhelms the negative Reynolds stress associated with the fundamental frequency thus retaining a positive stress throughout the flow. In fact, the slope of $\int\langle uv\rangle_{f/2} dy$ with X increased tremendously at the very same location at which $\int\langle uv\rangle_f dy$ became negative (i.e. at

X=350mm), At this very location the overall turbulence production for the ***TFS*** flow had its minimum (Fig. 1.1). This suggests that the coherent motion associated with the fundamental frequency transfers energy to the subhamonic and it may do so due to a resonance. The contribution of the 3fo/2 frequency to the Reynolds stress is negligible for all three types of excitation used, although its energy content is significant, particularly in the ***TFS*** case. This leads one to believe that the 3fo/2 mode does not interact with the mean motion but rather with the two forced waves.

6. Vorticity balance.

Before discussing further the role of the coherent structures in this flow and their effects on the vorticity distribution, one should verify that the phase locked and ensemble averaged vorticity field derived from the measured velocity field is indeed correct. Thus, the vorticity balance was tested. Reynolds decomposition of the equations of motion into steady and random components renders the turbulent energy budget that expresses the interaction between the mean motion and the turbulence through production term. Triple decomposition into mean, coherent and random motion (Hussain 1983), yields a coherent energy equation that explains the interaction between the coherent and the mean energy through production term; it also provides for the interaction between the coherent and the random components of energy through the inter-modal production term. However, this equation does not provide information about the interactions that occur among the coherent motions themselves, this can be provided by the vorticity equation. Thus, a vorticity balance will enable us. to explore the nonlinear wave interactions.

According to Hussain (1983), the rate of change of the mean vorticity is given by:

$$\frac{\overline{D}}{Dt}\Omega = \Omega_j \frac{\partial U_i}{\partial x_j} + \nu \frac{\partial^2 \Omega_i}{\partial x_k \partial x_k} + \frac{\partial}{\partial x_j}(\overline{u_{Ci}\omega_{Cj}} - \overline{u_{cj}\omega_{ci}})$$

$$+ \frac{\partial}{\partial x_j}(\overline{u_{ri}\omega_{rj}}) - \overline{u_{rj}\omega_{ri}})$$

Where the first term on the right side of the equation represents the stretching and twisting of the mean vorticity by the mean velocity gradients. The second term represents the viscous diffusion to the mean vorticity. The third term represents the time averaged interaction (i.e. stretching and convection) between the coherent vorticity and the coherent velocity fluctuations, while the fourth term does the same for the random motion.

Similarly, the substantial derivative of the coherent vorticity:

$$\frac{D\omega_{ci}}{Dt} = \omega_{Cj}\frac{\partial U_i}{\partial x_j} + \Omega_j\frac{\partial u_{Ci}}{\partial x_j} + \nu\frac{\partial^2 \omega_{Ci}}{\partial x_k \partial x_k} + \frac{\partial}{\partial x_j}(u_{Ci}\omega_{Cj} - \overline{u_{Ci}\omega_{Cj}})$$

$$-\frac{\partial}{\partial x_j}(\omega_{Ci}u_{Cj} - \overline{\omega_{Ci}u_{Cj}}) - \frac{\partial}{\partial x_j}(u_{Cj}\Omega_i) + \frac{\partial}{\partial x_j}(<u_{ri}\omega_{rj}> - \overline{u_{ri}\omega_{rj}})$$

$$-\frac{\partial}{\partial x_j}(<\omega_{ri}u_{rj}> - \overline{\omega_{ri}u_{rj}})$$

is balanced by the sum of the eight terms on the right side of the equation. Now however, the first term on the right side represents the stretching of the coherent vorticity by the mean velocity gradients while the second term represents the stretching of the mean vorticity by the coherent velocity gradients. The third term yields the viscous diffusion of the coherent vorticity. The fourth and fifth terms represent the residual coherent (after subtracting the mean) interaction between the coherent vorticity and the coherent velocity fluctuations. They again represent the stretching and convection of the coherent vorticity that is analogous to the third term in the mean vorticity equation. The sixth represents the convection of mean vorticity by the coherent eddies, while the seventh and eight terms the residual coherent (after subtracting the mean) interaction between the random vorticity and random velocity fluctuations

By assuming that the coherent motion is principally two-dimensional (2D) the streamwise component of the coherent vortices may be neglected. One may also assume that the influence of the random motion is secondary and negligible and therefore terms 1, 4 and the first portion of term 3 can be dropped from the mean vorticity equation. For the same reason, the terms 1, 2, 4, 7 and 8 on the right side of the coherent vorticity equation can also be neglected.

The rate of change of mean vorticity (left hand side of the mean vorticity equation) was calculated directly from the measured mean velocites for typical x locations and plotted using discrete symbols in Fig.6.1. The lines represent the same quantity that was calculated from the right side of the equation and required phase –locked and ensemble averaged input. The good agreement between the two sets of data indicates that the measurements and the assumption of two-dimensionality of the coherent structures are valid. The calculations suggested that the viscous diffusion term can also be neglected thus, the rate of change of the mean vorticity is only caused by the time-averaged convection of the coherent vorticity by the coherent velocity. In other words, the changing distribution of the mean vorticity across the flow and consequently the spreading rate of the entire mean velocity field is caused by the non-linear interaction between coherent motions.

The calculations based on the coherent vorticity equation were not as satisfactory, particularly near the borders of the mixing layer with the respective uniform streams and near the center of the mixing layer. Thus, the results plotted in Fig. 6.2 are for two selected Y locations on each side of the mixing layer only; they contain however, all

three data sets: ***SF, TFW, TFS.*** The agreement between the calculations and the measurements (i.e. representing both sides of the coherent vorticity equation) is qualitatively reasonable. The discrepancies attributed to lack of two-dimensionality and to the terms representing the random motion (terms 7 and 8) that probably should not have been neglected. Since the viscous diffusion term was again negligible, the rate of change of the coherent vorticity is balanced by terms 5 and 6 in the equation (i.e. the convection of coherent and mean vorticity by the coherent eddies).

7. Coherent vorticity.

The isodynes (vorticity contours) plotted in Fig. 7.1 were calculated from the two-dimensional, phase locked and simply, ensemble-averaged data. They show the interactions between adjacent, coherent vortices and they provide a visual basis for comparing the three experiments, ***SF, TFW, TFS***. The time-averaged results of these interactions are rooted in the vorticity balance described above. Only the most relevant isodynes are shown in Fig. 7.1 because some of this data was published elsewhere together with the associated streak lines (Wygnanski & Weisbrot 1988). An attempt was made to sharpen those images by using the temporal pattern recognition technique (Zhou et al, 1995) but the improvement in the results did not warrant the added complexity.

The coherent structures in the ***SF*** case (for X>500mm, corresponding to the location where the linear amplification of the disturbances at the fundamental frequency ceases) are well represented by a single row of vortices, whose strength diminishes with increasing X. These vortices are equally spaced in the direction of streaming and are aligned with the mean center of the flow (i.e. $Y_{0.5}$). For the ***TFW*** case, adjacent vortices are staggered slightly around the mean center line due to the imposed subharmonic perturbation. This leads to a mutual induction that results in a decrease of the stream wise distance between them as they proceed downstream (compare Fig.7.1b numbers 4 & 5), leading to possible pairing beyond the measurement domain. The lateral displacement of adjacent pair of vortices in the ***TFS*** case is much larger, even at small values of X, and that enables their amalgamation within the measurement domain (Fig. 7.1c numbers 5 & 6). The large, lateral displacement of these eddies causes the observed distortions in the mean velocity (Fig. 1.3), and results in the peculiar distribution of amplitudes of the leading frequencies contained in these coherent structures (see Fig. 5.3). Since the levels contained in the coherent parts of the motion dominate the flow they may even be observed in the turbulent intensity distribution shown in Fig. 2.2c.

The vortices displaced toward the high velocity side (upward in Fig 7.1) in the ***TFW*** case retain their strength much further downstream than the vortices displaced downward (i.e. toward the low velocity side). However, the relative strength of adjacent vortices in the ***TFS*** case oscillates with increasing streamwise distance. This suggests that there is a periodic exchange of vorticity and presumably energy between such pair of vortices during their amalgamation process. Initially, the strength of the vortex that is displaced upward increases with X while the vorticity contained in the one displaced downward (toward the lower velocity side in Fig. 7.1c) is quickly depleted (compare numbers 2, 3 & 4 in Fig. 7.1c). The process is reversed for X>1200mm (see numbers 5 & 6 in Fig. 7.1c).

The Reynolds stress distribution is also closely related to the shape and inclination of the isodynes as was suggested by Browand & Ho (1983) and by Hussain (1983). When an eddy represented by a closed vorticity contour is tilted backward (i.e. it is advanced more on the low velocity side than on the high velocity side), the Reynolds stress that it generates is positive. When it is tilted forward, its contribution to the Reynolds stress is negative. Amplified, wavy perturbations are associated with vortices that are tilted backward while decaying ones are always tilted in the forward direction (Michalke 1964, Wygnanski & Weisbrot 1988). One may also filter the phase locked and ensemble-averaged signals and determine the frequency that dominates the isodynes and whether that mode decays or amplifies. For example: eddy number 1 in the ***SF*** case (Fig. 7.1a) is amplified while 2 starts to decay and the decay rate of 3 is even larger. In the ***TFW*** flow eddy number 1 is amplified, 2 is almost neutral while the fundamental modes 3 & 4 (shown as single vorticity concentrations in Fig. 7.1b) that are further downstream, decay. The combination of the two vortices (Fig. 7.1b number 5) indicates amplification at the subharmonic frequency since the line connecting the two centers is tilted backward. A similar observation can also be made for the ***TFS*** experiment where the rate of amplification of the subharmonic mode increases up to the maximum at vortex pair 5 (angle of inclination approximately 45 degrees) and then decreases at large X (4, 5 & 6 in Fig. 7.1c).

The relation between the inclination of a coherent vortex to the flow direction (marked by the angle ϕ in Fig. 7.1b & 7.2b) and the coherent Reynolds stress that it generates may be quantified by assuming that such an eddy conserves its angular momentum. Consequently: $(u'^2+v'^2)r = C$, where u' and v' are the coherent velocity components and r is the distance of the typical point on the control surface from the center of the vortex (Fig.7.2b). C is a constant defining the intensity of the circulation in the vortex.

Assuming that only the orientation of the vortex varies during its movement downstream, the coherent velocity induced by such a vortex will not change for an observer moving with the vortex. Thus, the relation between the u'v' and the vortex orientation can be found by considering any point that is fixed on the vortex. For simplicity, a point located at the end of the minor axis (see point A marked on Fig. 7.2b) is chosen for this purpose.

$$\text{Thus: } u' = \sqrt{\frac{C}{r}}\sin\phi\,; -v' = \sqrt{\frac{C}{r}}\cos\phi\,; \text{ and } -u'v' = \frac{C}{2r}\sin(2\phi)$$

$$\text{Consequently, } \int_{-\infty}^{\infty}\int_{-\infty}^{\infty}(-u'v')dxdy = \frac{C}{2}\sin(2\phi)\int_{-\infty}^{\infty}\int_{-\infty}^{\infty}\frac{1}{r}dxdy \qquad \text{(A)}$$

For a particular vortex, the maximum or minimum integral of the coherent Reynolds stress should occur wherever $\sin(2\phi)=\pm 1$ or the inclination of the vortex is: $\phi=\pm 45^0$.

$$\text{Thus: } \left[\int_{-\infty}^{\infty}\int_{-\infty}^{\infty}(-u'v')dxdy\right]_{max} = \frac{C}{2}\int_{-\infty}^{\infty}\int_{-\infty}^{\infty}\frac{1}{r}dxdy \qquad \text{(B)}$$

Dividing equation A by B gives: $\phi = \frac{1}{2}\arcsin[\frac{\int_{-\infty}^{\infty}\int_{-\infty}^{\infty}(-u'v')dxdy}{(\int_{-\infty}^{\infty}\int_{-\infty}^{\infty}(-u'v')dxdy)_{max}}]$

The integration along X can be replaced by the integration over time that yields:

$$\phi = \frac{1}{2}\arcsin[\frac{\int_{-\infty}^{\infty}(-\overline{u'v'})dy}{(\int_{-\infty}^{\infty}(-\overline{u'v'})dy)_{max}}]$$

The calculated inclination angles of the fundamental coherent vortices based on the Reynolds stress (Fig.5.4c) are shown in Fig.7.2c and are compared to the vorticity contours in Fig.7.2a. For the ***SF*** case, the fundamental component of the Reynolds stress is maximum at X=300mm while vanishing at X=550mm before attaining a minimum negative stress at X=700mm. The corresponding calculated inclination angles of the isodynes (Fig. 7.2c) corroborate these findings ϕ=+45^0 at X=300mm, ϕ=0^0 at X=550mm and ϕ=-45^0 at X=700mm. One may also compare the calculated values with isodynes (considering the fundamental only) in the ***TFW*** and ***TFS*** cases. The good agreement between the two very different sets of measurements, suggest that the correlation between them is high.

If, however, one concerned with the coherent Reynolds stress of the subhamonic one may consider adjacent pairs of vortices as shown in Fig. 7.1b & c (numbers 4 & 5) or filter the coherent vorticity so it includes the subharmonic only. In the ***TFS*** case the maximum coherent Reynolds stress at the subharmonic frequency occurred at X=1100mm and it corresponds to $\phi_{fo/2}$ = +45^0 (see Fig.7.1c number 5).

8. The conditions for resonance and the definition of a dominant mode.

The oscillatory interchange of the intensity of circulation between adjacent pairs of vortices or between the two vortices within a pair in the ***TFS*** flow (Fig. 7.1c) suggest that a resonant interaction might have taken place between the fundamental and the subharmonic. Furthermore, in many instances (for the ***SF*** excitation in particular), the energy contained within the coherent structures increases or decreases depending on the sign of coherent Reynolds stress (fig. 5.4c). It implies that the coherent eddies exchange energy with the mean motion, mostly extracting energy from it, via the production term <uv>dU/dY. This however, is not always so as was observed for the ***TFS*** excitation (Fig 5.4b & c). Here, the energy contained in the fundamental mode increases in the direction of streaming (for X>380mm) despite the fact that the shear stress associated with this mode is negative between X=380mm and 1060mm. On the other hand, the energy contained in the fundamental mode follows the positive production term and increases beyond X=1060mm. The mismatch between the increase in the energy contained by a

specific mode and the production term for this mode implies that the energy comes from sources other than the mean motion and this again suggests a resonance.

The standard conditions for triad resonance in parallel shear flow that is concomitantly excited by two wavy disturbances, *fo and fo/2* are:

$$\alpha_{res} = \alpha_{fo} \pm \alpha_{fo/2}$$
$$\beta_{res} = \beta_{fo} \pm \beta_{fo/2}$$

where β is the frequency and α is the wave number. Whenever the instabilities are evolving in space α is complex ($\alpha = \alpha_r + i\alpha_i$) while β is real and determined by the excitation frequency. In the present experiment β_{res} might be associated with the subharmonic, *fo/2* (that is also the difference between the imposed frequencies), or with their sum *3fo/2*. In order that the two primary waves will exchange energy between them, they have to travel together i.e. their phase velocity, $c_{ph} = \beta/\alpha_r$, has to be identical over some region. In parallel flows, excited at constant frequencies, this may be a frequent occurrence because α is constant across the flow [i.e. $\alpha = \alpha(x)$ only], but in a divergent mean flow of the kind considered presently, the regions of possible interaction are more limited since $\alpha = \alpha(x,y)$. Another complicating factor is the fact that energy can be exchanged between the coherent eddies and the mean flow that in turn responds by changing its rate of divergence in the direction of streaming and/or by getting distorted.

The phase velocities of the dominant disturbances were calculated for the entire flow field and for the three experiments considered. A sample of those c_{ph} representing the variation of the <v> component with x are plotted in Fig. 8.1 for three locations across the flow: on the high velocity side (Y≈100mm), in the center (Y≈0) and on the low velocity side (Y≈-110mm). The <v> component was selected because it is the most amplified component of the flow, its amplitude is large in the central region of the mixing layer and it does not reverse its phase in the center. The phase velocity of the fundamental mode that is the only frequency of significance in the ***SF*** experiment, is approximately constant everywhere and roughly equal to: $U_c=0.5(U_1+U_2)$. The phase velocity of the fundamental mode in the ***TFW*** case is also constant throughout the flow but the other two modes oscillate around it. These oscillations diminish with x in the central region of the flow (i.e. atY=-5mm) and they are hardly significant beyond x>1000mm (see Fig. 8.1b). On the high speed side of the flow all three modes travel together up to x=1200mm whereupon the *3fo/2* mode undergoes a rapid acceleration (Fig. 8.1a). On the low velocity side of the flow the three waves locked in phase at x>800mm. For 800<x<1200 there is a reasonable lock-in among all three waves across the entire width of the flow. In this region however, the mean flow is slightly contracting (Fig. 1.1) due to the negative production associated with the decaying fundamental mode (Figs. 5.4c).

The ordinate in fig. 8.2 represents the rate of amplification of a given mode defined by $\theta d/dx\{log[\int(<v>^2 + <u>^2)_f dY]/ [\int(<v>^2 + <u>^2)_f dY]_o\}$. When a single wave develops in a linear manner due to the instability of the mean motion this quantity is analogous to $-\alpha_i \theta R$. The fundamental mode amplifies and decays in a manner consistent with a linear model. During its decay (for x>850mm) it probably transfers some energy to the mean motion because the production term of the fundamental is negative and the mean flow

responded by reversing its lateral rate of spread (fig. 1.1). A reduction in the energy thickness (that behaves like θ) indicates a gain in the mean energy.

In ***TFW***, the energy contained in the subharmonic mode keeps increasing (fig. 5.4) and its rate of increase does not diminish between 800 and 1200mm from the origin (fig. 8.2). A linear model would have predicted a reduction in that rate which would presumably be parallel to the reduction in the fundamental, f_0. The $3f_0/2$ component lost energy in this x interval (fig. 5.4), as it also appears in figure 8.2.Thus, in this range of stream-wise locations the amplification of f_o and $f_0/2$ is enabled by a transport of energy from the mean flow (through the production of the fundamental) and by the decay the $3f_0/2$ mode. The incoherent motion also decreases in intensity in this region (i.e. for $800<x<1200$mm) eliminating the possibility of energy transfer to the random, smaller scale eddies. Thus the dominant mode, over most of the measurement domain (for $x<1300$mm, see fig. 5.4b), is the fundamental mode that behaves in a manner reminiscent of the linear development.

Under ideal (linear) development, the subharmonic mode should have attained its largest rate of amplification where the fundamental becomes neutrally stable (i.e. around x = 850mm; Fig. 8.2a) It could have then amplified further (Kelly 1967) if it were to receive energy from the fundamental. This is probably not the case in this flow, since the rate of amplification of the subharmonic remained constant in this region (i.e. for $850<x<1300$) and the total mean energy did not change as well (the rate of spread of the mixing layer stopped). The resonance proposed by Kelly might have occurred at larger distance (i.e. at $x>1300$mm) where the rate of decay of the fundamental and the rate of amplification of the subharmonic have both increased. The two modes traveled together (Fig. 8.1 a-c) and during this interval the amplitude of the subharmonic increased tremendously (Fig. 5.4). The most plausible explanation to this exchange of energy is resonance.

In contrast to the ***TFW*** experiment the phase velocity of subharmonic in the ***TFS*** case keeps almost constant throughout the entire measurement domain. The phase velocities of f_o and $3f_o/2$ are almost identical to the subharmonic on both sides of the flow, but differ from it in the central region for $x>850$mm (fig. 8.1e). Around this streamwise location, the decay rates of both of these modes attained their maximum. The fundamental mode starts to amplify for $x>1000$mm, at this x its phase velocity is sufficiently different from the subharmonic's and it can no longer transfer energy to it. The $3f_o/2$ mode follows suit around x=1200mm and resumes its amplification while the amplification rate of the subharmonic decreases in this region (fig. 8.2b). Consequently the subharmonic appears to be the dominant wave in the ***TFS*** experiment.

Yao (1998) suggested that the mean flow is involved in the resonance and it could be considered as a wave of zero frequency and an infinite wave length. It contributes to the energy transfer between the fundamental and the subharmonic and sometimes has a role of a catalyst in the process. Therefore, the production term of an individual mode (e.g. $<uv>_{f_o}dU/dy$) does not conflict with the concept of resonance. Consequently the integrated production rates of f_o and of $3f_o/2$ across the flow are plotted on figure 8.2. The spectra presented in fig. 4.1 indicate that f_o is the dominant mode in the ***TFW*** experiment. This dominance is shared among all three major waves ($f_o/2$, f_o, & $3f_o/2$) near

the origin of the ***TFS*** experiment but it ends with the dominance of $f_o/2$ in the last 50% of the measurement domain.

9. CONCLUDING REMARKS

The turbulent mixing layer is very sensitive to external, two-dimensional excitation because the momentum transport across it is mostly coherent. In some instances more than 90% of the ensuing Reynolds stress is even contained within the excitation frequency. Furthermore by exciting the flow at two frequencies, a fundamental and a subharmonic, the resulting Reynolds stresses remain large and coherent throughout the test section. This is not the case when the flow is excited at a single frequency. Calculations based on the two-dimensional mean momentum and vorticity equations suggest that the mean flow and the large coherent eddies are predominantly two-dimensional. Reasonable mean and coherent vorticity balances were attained by assuming both components to be two-dimensional and totally neglecting the influence of random motion. This opened the possibility of correlating the coherent Reynolds stresses to the deformation and orientation of the spanwise coherent vortices.

The dramatic increase in Reynolds stress resulting from simultaneous excitation at the fundamental and subharmonic frequencies is associated with a resonance phenomenon that extracts energy from the mean motion or from the fundamental excitation frequency depending to a large extent on the level of the excitation. When the level of the subharmonic frequency is high it quickly dominates the flow and the measure of this dominance may be assessed by the linear-like behavior of this mode. This might be tested by its relation to the rate of spread of the mean flow. For a mean velocity profile that can be approximated by a hyperbolic tangent {i.e. U=1/2[1+tanh(y)]}, a linear perturbation attains its maximum amplitude (i.e. becomes neutrally stable) where $f\theta/U_c=0.08$. This number was reached at x=850mm for the ***TFW*** case where the dominant frequency considered in the above equation was fo. The same number was attained near the end of the measurement domain (around x=1350mm) for the ***TFS*** case but the dominant frequency considered in this case was $fo/2$. Therefore the quantity $f\theta/U_c=0.08$ may serve as a criterion for the determination of the dominant mode in a flow excited by a multitude of periodic perturbations. All the results collapse approximately onto a single curve (Fig. 9.1b) when the measured $f\theta/U_c$ is scaled with $Rf(X-Xo)/Uc$ where f is the dominant frequency, Uc is the measured phase velocity at the dominant frequency and $R=(U_1-U_2)/(U_1+U_2)$.

The practical advantage of exciting the flow at two frequencies simultaneously becomes self evident when one assumes that the dimensionless saturation thickness, based on the predominant frequency, remains unchanged. The excitation at the fundamental frequency is advantageous at small X because the mean flow amplifies this frequency more rapidly than its subharmonic and it responds by spreading faster (Fig.9.1a). However, if the subharmonic has a substantial amplitude at the saturation location of the fundamental, it may extract energy from it through resonance and thus dominate the rate of spread of the mixing layer as long as it did not reach its new dimensioless saturation value (Fig. 9.1b). This technique enables the mixing layer to become twice as wide at a prescribed distance from its origin. Since the large coherent

eddies control the scalar transport and the rate of chemical reaction (Roberts, 1985)the concomitant excitation of the flow at both frequencies has its payoffs. It also should have an impact on the effectiveness of the control of separation by periodic excitation because it depends on the rate of entrainment of ambient fluid by the mixing layer near a solid surface.

ACKNOWLEDGEMENSTS

This research was supported by AFOSR grant number F49620-96-1-0187 monitored by Dr.J.McMichael. The authors also wish to thank Mr.I.Weisbrot who measured the three sets of the mixing layer data which were adopted as the data base of this paper.

REFERENCES

Acton,E. 1976 The modeling of large eddies in a two-dimensional shear layer. J.Fluid Mech. **76**,561.

Ashurst,W.T. 1979 Numerical simmulation of turbulent mixing layers via vortex dynamics. In *Turbulent shear flows*, **1**, 402.

Browand, F.K. & Weidman, P.D. 1976 Large scales in the developing mixing layer. J.Fluid Mech. **76** 127.

Browand, F.K. and Ho, C.M., 1983 The mixing layer: an example of quasi two-dimensional turbulence J.de Mecanique

Brown, G.L. & Roshko,A. 1974 On density effects and large structure in turbulent mixing layers. J. Fluid Mech. **64**, 775.

Corcos, G.M. & Sherman, F.S. 1984 The mixing layer: deterministic models of a turbulent flow. Part 1. Introduction and the two-dimensional flow. J.Fluid Mech. **139**, 29.

Crighton, D. G. and Gaster, M. 1976. "Stability of Slowly Diverging Jet Flow," Journal of Fluid Mechanics 77, 397.

Fiedler, H.E, Dziomba, B., Mensing, P., and Rosgen, T. 1981 Initiation, evolution and global consequences of coherent structures in turbulent shear flows. Lecture notes in Physics vol. **136**, 219

Fiedler,H.E. & Mensing, P. 1985 The plane turbulent shear layer with periodic excitation. J.Fluid Mech. **150**, 281.

Gaster, M., Kit, E. & Wygnanski, I. 1985 Large scale structures in a forced turbulent mixing layer. J. Fluid Mech. **150**, 23.

Ho, C.M. & Huang,L.S. 1982 Subharmonics and vortex merging in mixing layers. J.Fluid Mech. **119**, 443.

Hussain, A.K.M.F. 1983 Coherent structures — reality and myth. Phys. Fluids **26**, 2816.

Inoue,O. & Leonard, A. 1987 Vortex simulation of forced/unforced mixing layers. AIAA Paper 87-0288.

Inoue, O. 1989 Artificial control of turbulent mixing layers. proceedings of Second IUTAM Symposium on Structure of Turbulence and Drag Reduction. Zurich, Switzerland, July 25-28, 1989.

Inoue, O. 1992 Double-frequency forcing on spatially growing mixing layer. J. Fluid Mech. **234**, 553.

Katz, Y., Nishri, B., and Wygnanski, I., 1989, The delay of turbulent boundary-layer separation by oscillatory active control, AIAA Paper 89-0975, also Phys.Fluids A, 1, 179.

Kelly, R.E. 1967 On the stability of an inviscid shear layer which is periodic in space and time. J.Fluid Mech. **27**, 657.

Michalke,A. 1964 On the inviscid instability of the hyperbolic tangent velocity profile. J.Fluid Mech. **19**, 543.

Monkewitz,P.A. & Huerre,P. 1982 The influence of velocity ratio on the spatial instability of mixing layers. Phys. Fluids **25**, 1137.

Neuburger, D., and Wygnanski, I. 1988,"The use of a Vibratting Ribbon to Delay Separation on Two dimensional Airfoils", Proceedings of Air Force Academy Workshop on Separated Flow", F.J. Seiler Research Labs. Rep. TR-88-0004,.

Oster,D., Wygnanski,I. Dziomba,B. & Fiedler,H. 1978 The effects of initial conditions on the two-dimensional mixing layer. Lecture Notes in Physics. **75**, 48.

Oster,D. and Wygnanski,I. 1982 The forced mixing layer between parallel streams, J. Fluid Mech. **123**, 91.

Patnaik,P.C., Sherman, F.S. & Corcos,G.M. 1976 A numerical simulation of Kelvin-Heimholtz waves of finite amplitude. J.Fluid Mech. **73**, 215.

Riley,J.J. & Metcalfe,R.W. 1980 Direct numerical simulation of a perturbed turbulent mixing layer. AIAA Paper 80-0274.

Roshko,A. 1976 Structure of turbulent shear flows: a new look. AIAA J. **14**, 349.

Roberts, F.A. (1985) Effects of a periodic disturbance on structure and mixing in turbulent shear layers and wakes, Ph.D. thesis California Institute of Technology, Pasadena CA.

Weisbrot, I. And Wygnanski, I. 1988 On coherent structures in a highly excited mixing layer. J.Fluid Mech. **195**, 137.

Winant,C.D. & Browand,F.K. 1974 Vortex pairing, the mechanism of turbulent mixing layer growth at moderate Reynolds number. J. Fluid Mech. **63**, 237.

Wygnanski, I. & Fiedler, H.E. 1970 The two-dimensional mixing region. J.Fluid Mech. **41**, 327.

Wygnanski,I., Fiedler, H., Oster,D. and Dziomba,B. 1979 On the perseverance of a quasi-two-dimensional eddy structure in a turbulent mixing layer. J.Fluid Mech. **93**, 325.

Wygnanski,I. And Petersen,R.A. 1987 Coherent motion in excited free shear flows. AIAA J. **25**, 201.

Wygnanski,I. And Weisbrot,I. 1988 On the pairing process in an excited plane turbulent mixing layer. J.Fluid Mech. **195**, 161.

Yao,L.S. 1998 A resonant wave theory. Submitted to Int. J. of Heat & Mass Transfer.

Zhang, Y.Q.; Ho, C.M.; Monkewitz, P. 1984 The mixing layer forced by fundamental and subharmonic.. Proceedings of IUTAM Symposium on Laminar-Turbulent Transition in Novosibirsk, USSR, July 9-13, 1984.

Zhou M.D., Heine,C. and Wygnanski I. 1996 The effects of excitation on the coherent and random motion in a plane wall jet. J. Fluid Mech. **310**, 1.

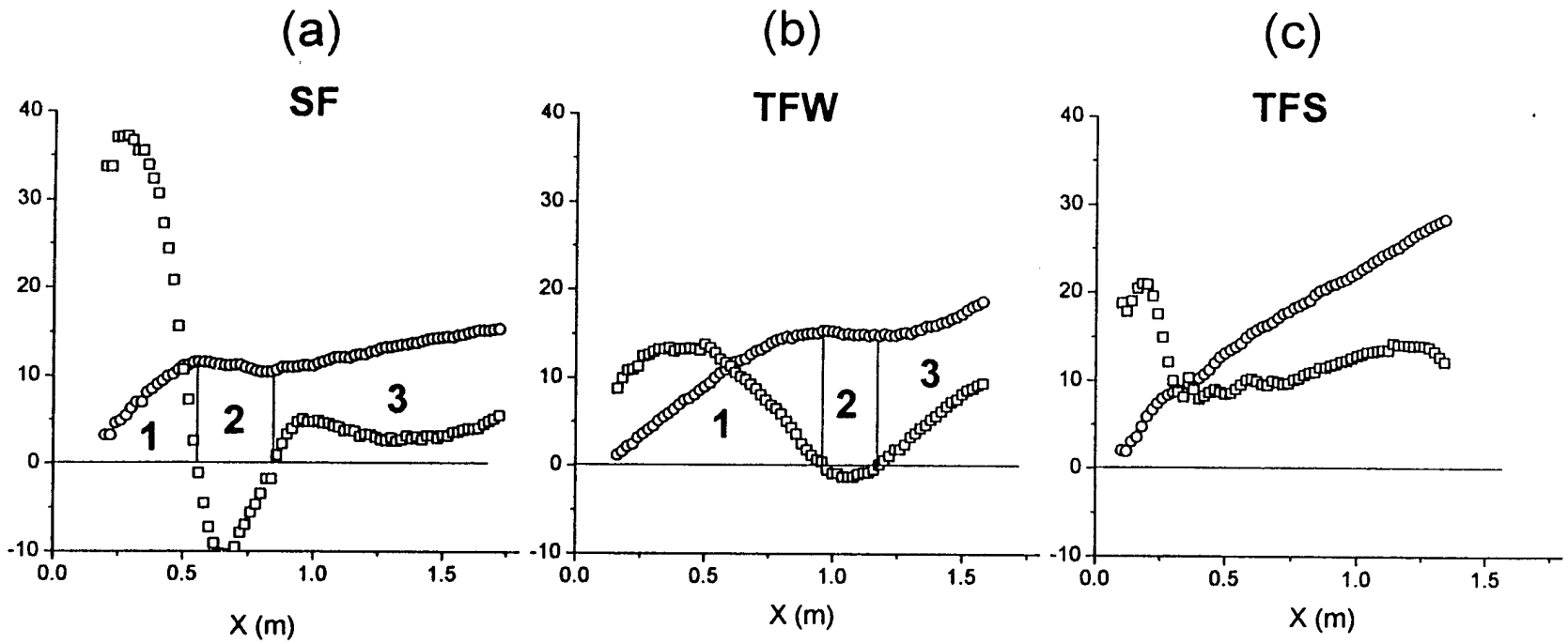

○ momentum thickness θ, mm

□ $\int \overline{u'v'} \frac{\partial U}{\partial y} dy / 50, (m^3 / \sec^3)$

Fig.1.1 Momentum thickness and integration of production across layer

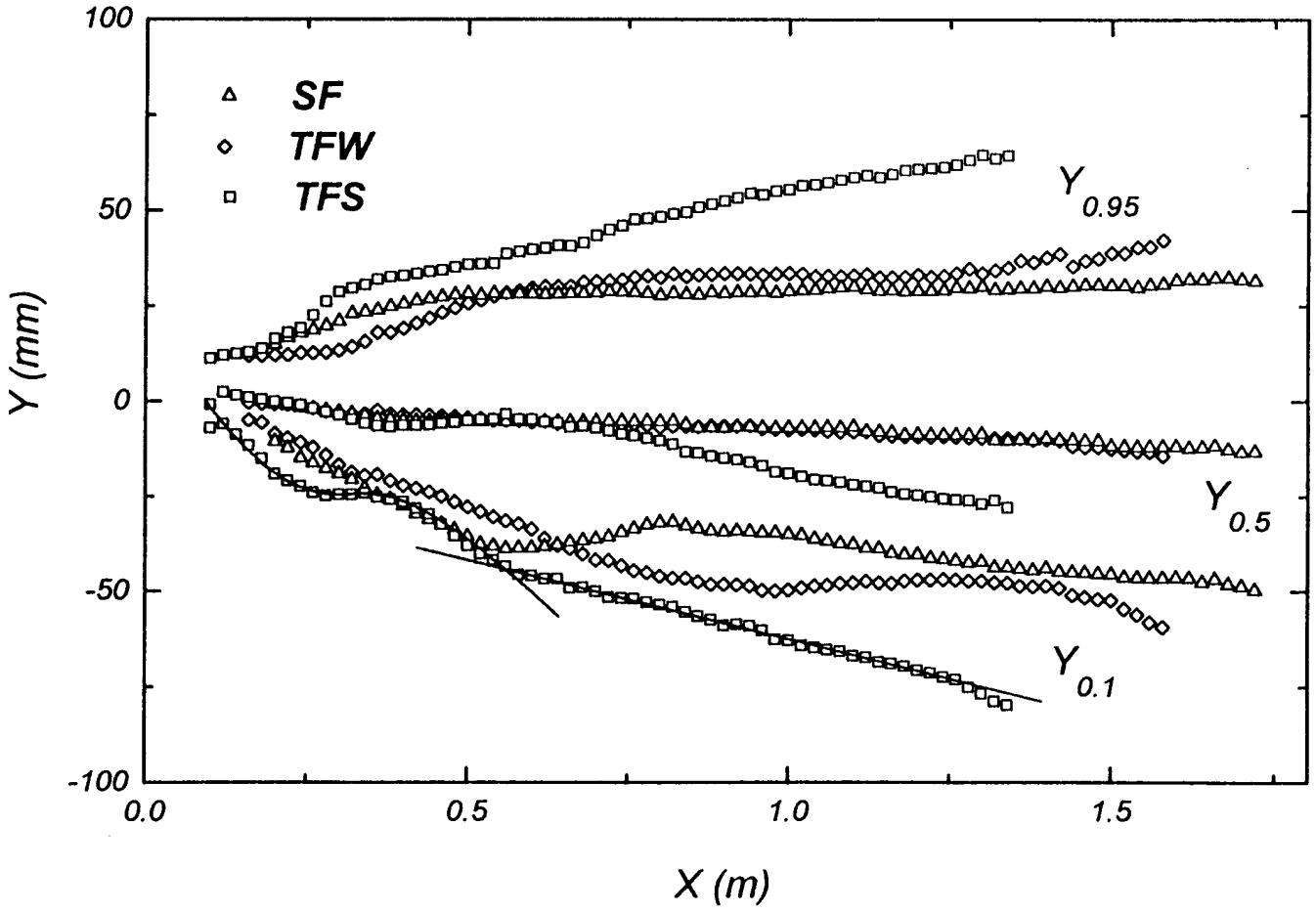

Fig.1.2 Streamwise distribution of the boundary

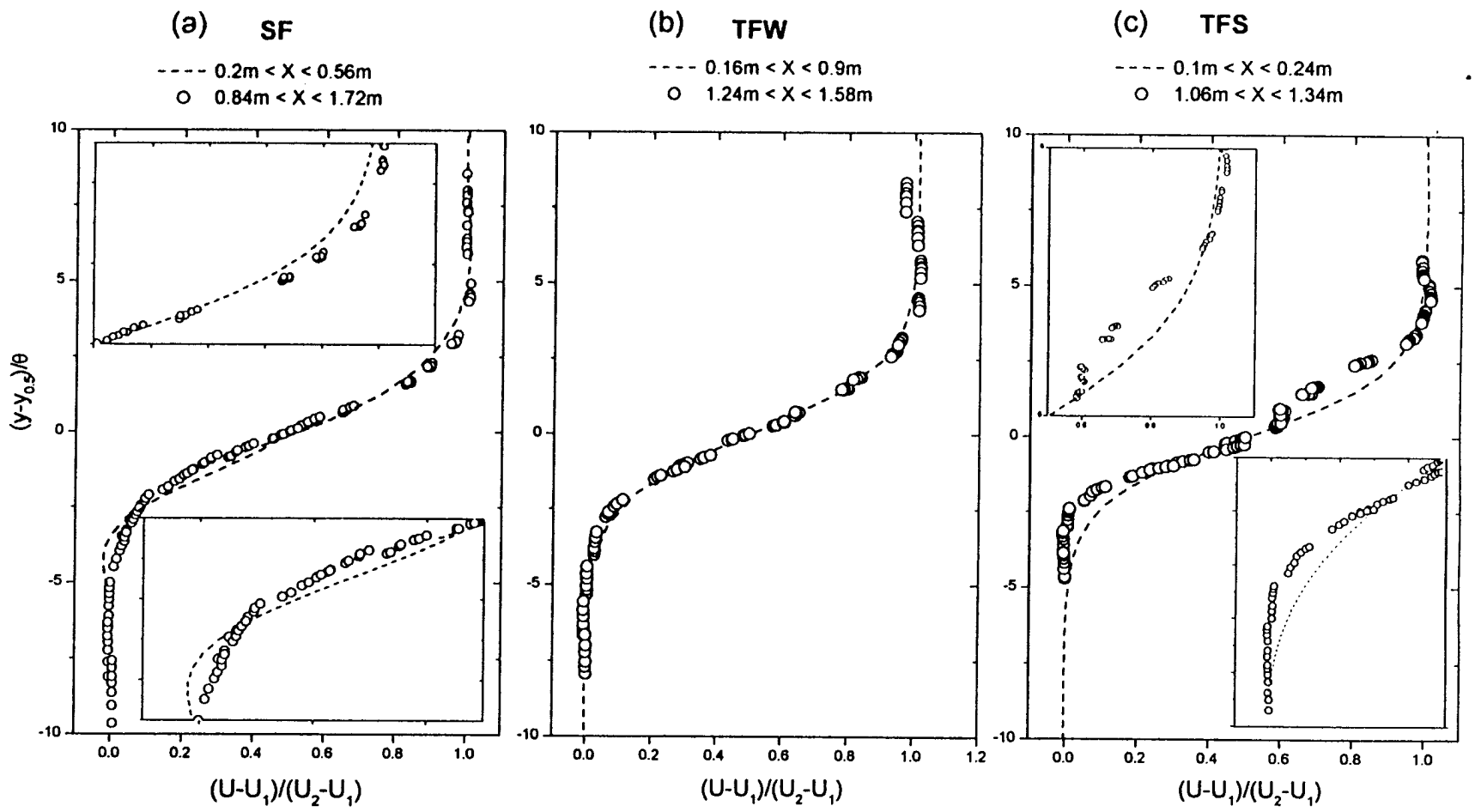

Fig.1.3 Comparison between upstream and downstream regions of the normalized mean velocity profiles.

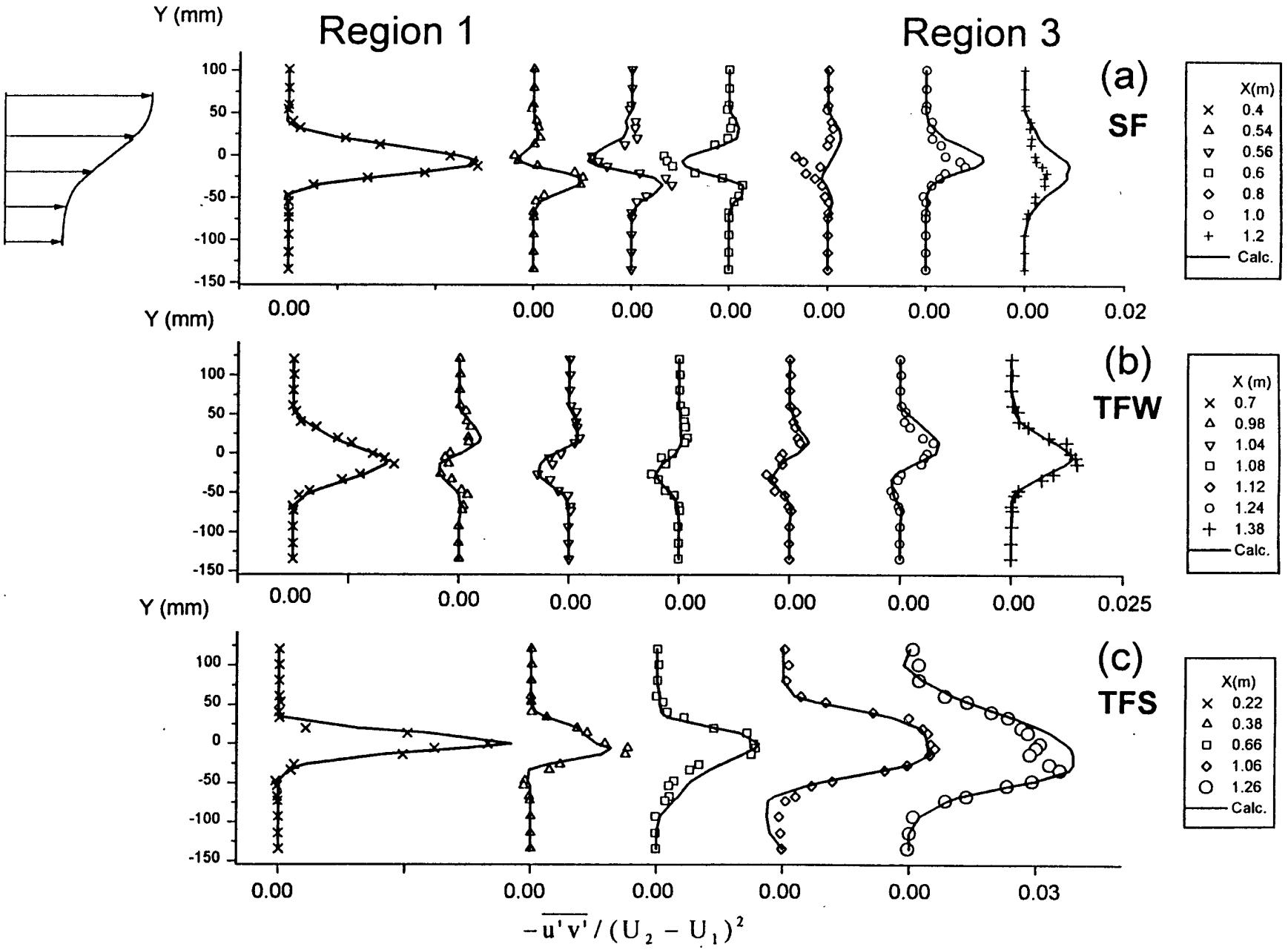

Fig.2.1 Reynolds stress distribution

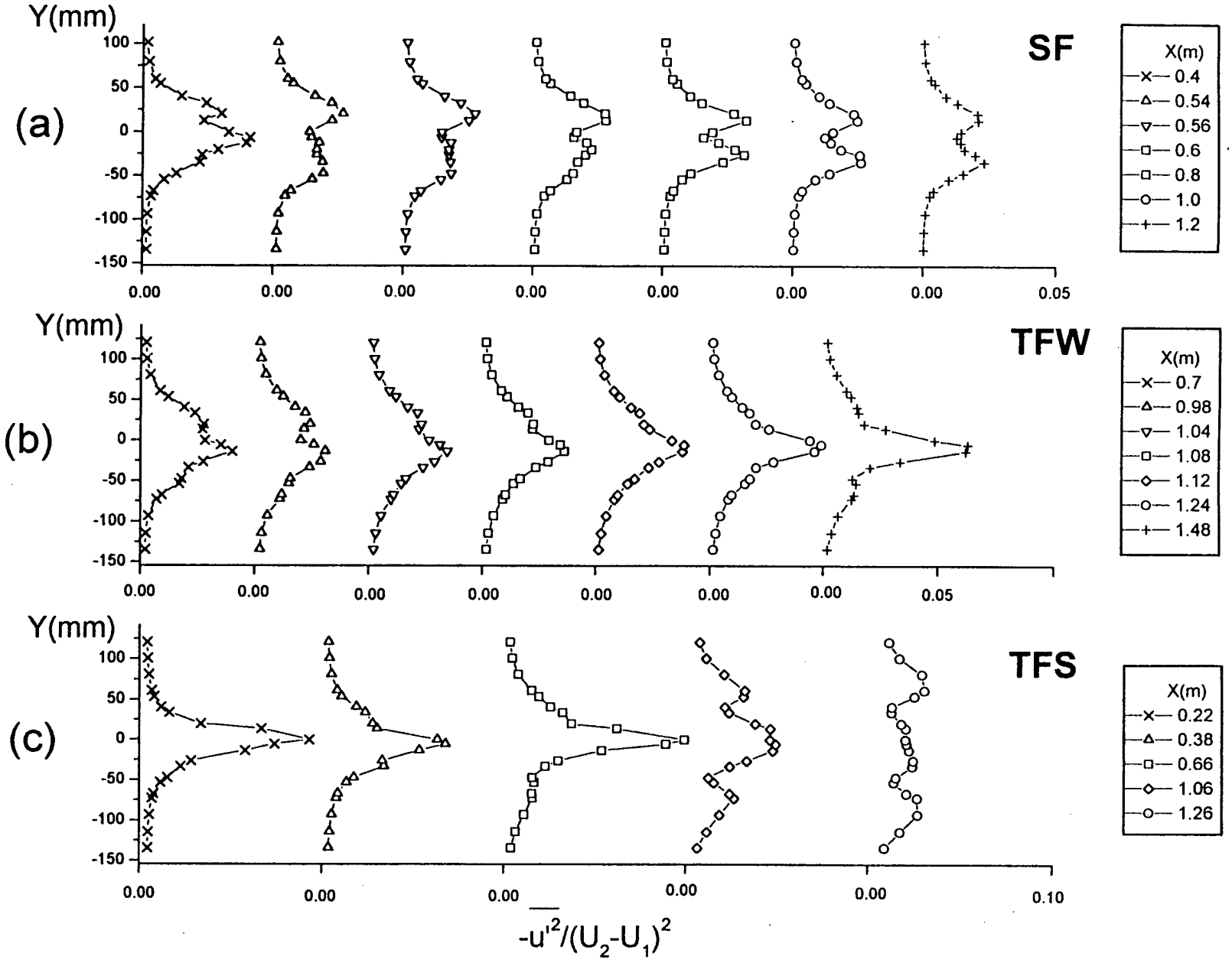

Fig.2.2 Turbulence energy distribution --- u component

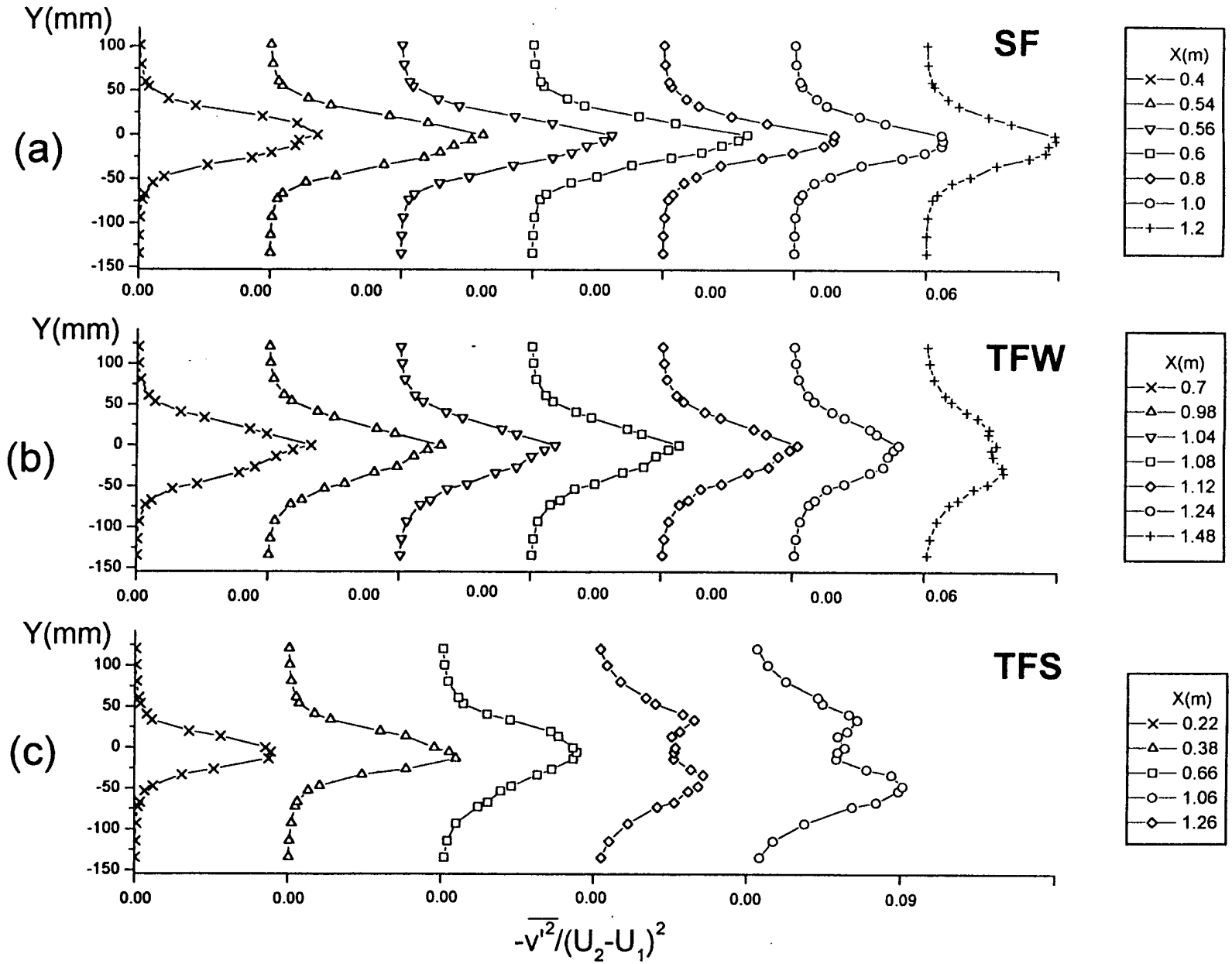

Fig.2.3 Turbulence energy distribution --- v component

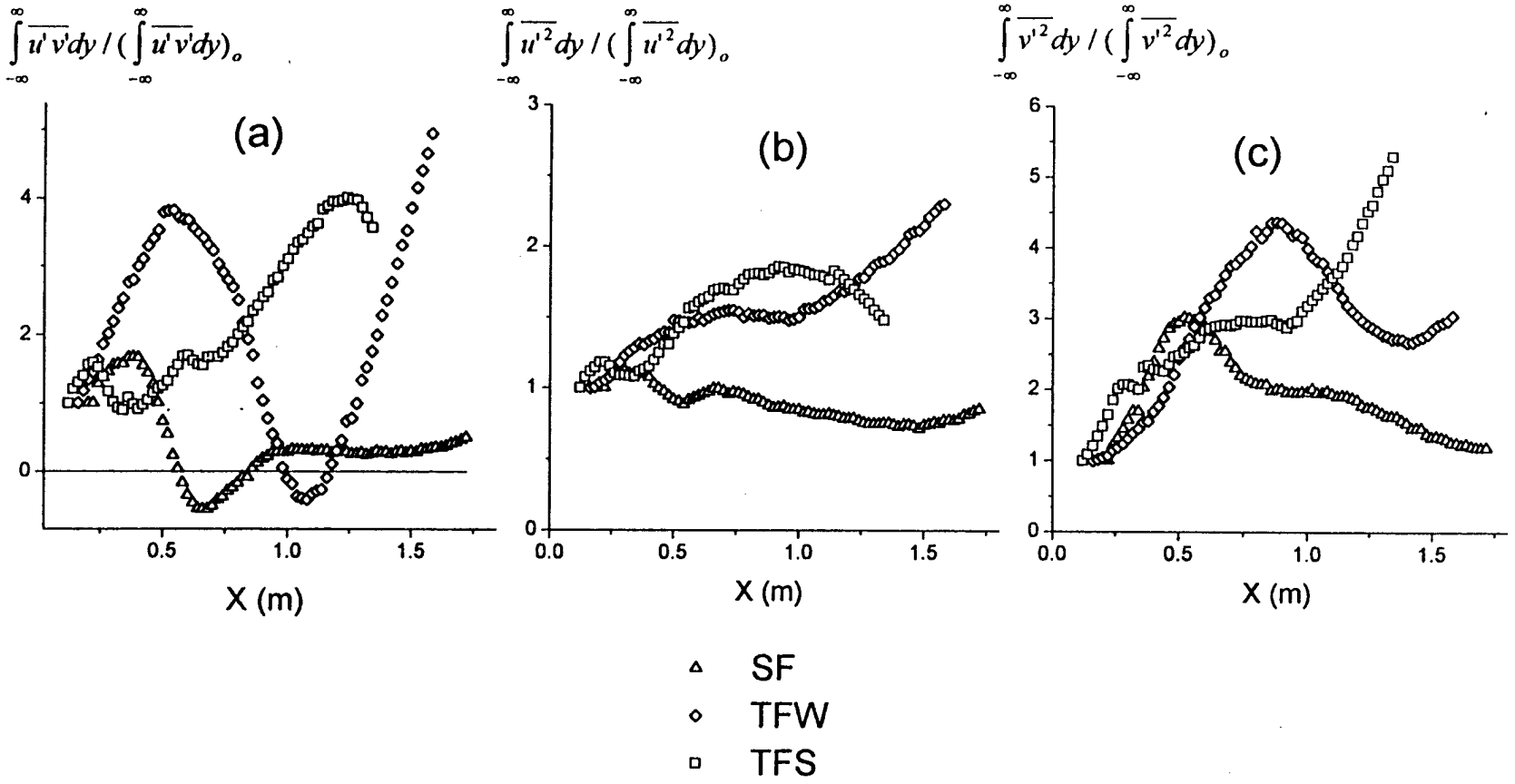

Fig.2.4 Integration of turbulence quantities across layer

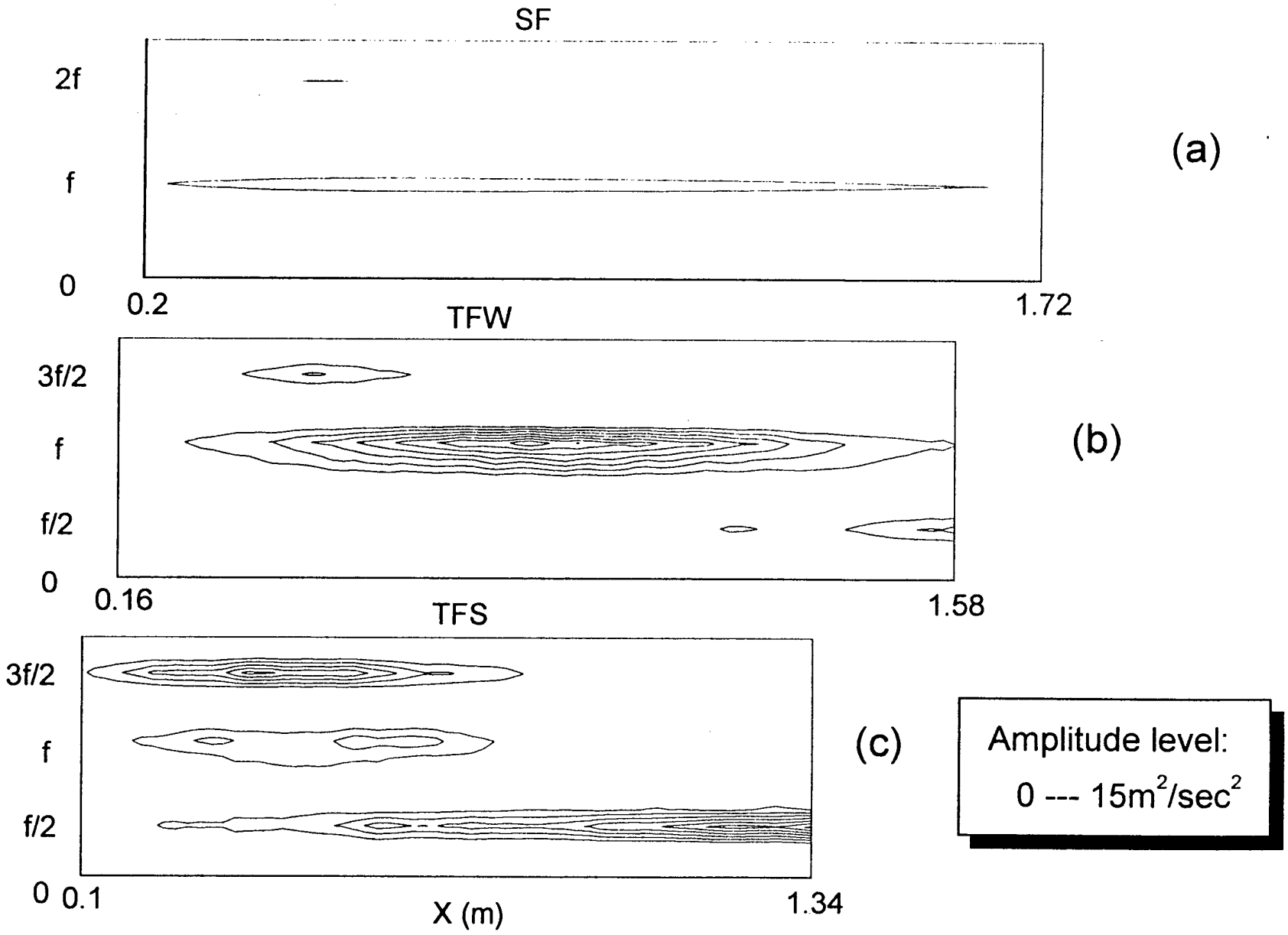

Fig.4.1 Power Spectra of the turbulence energy (v component)

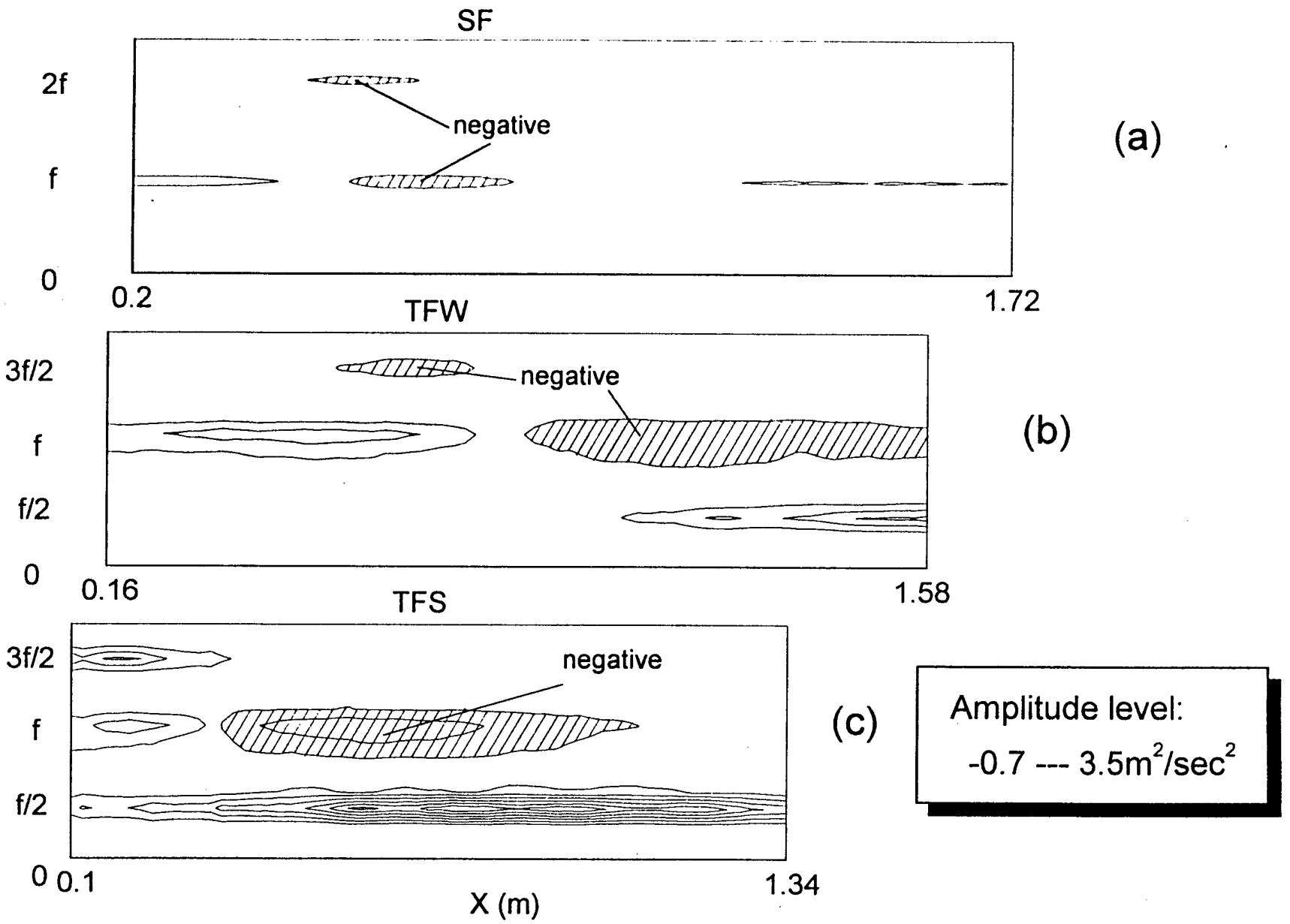

Fig.4.2 Spectra of Reynolds shear stress

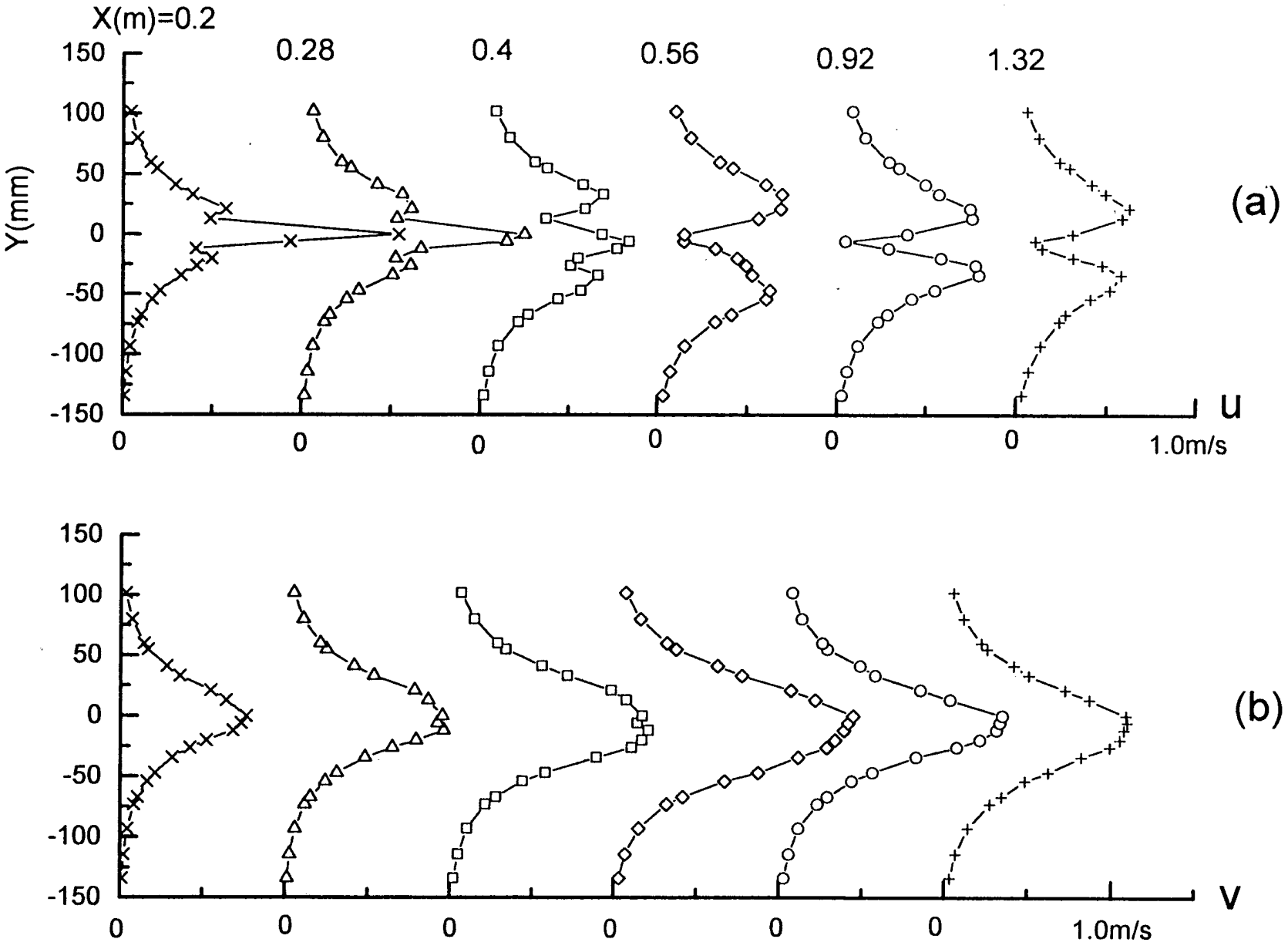

Fig.5.1 Amplitude distribution of the fundamental disturbance (SF)

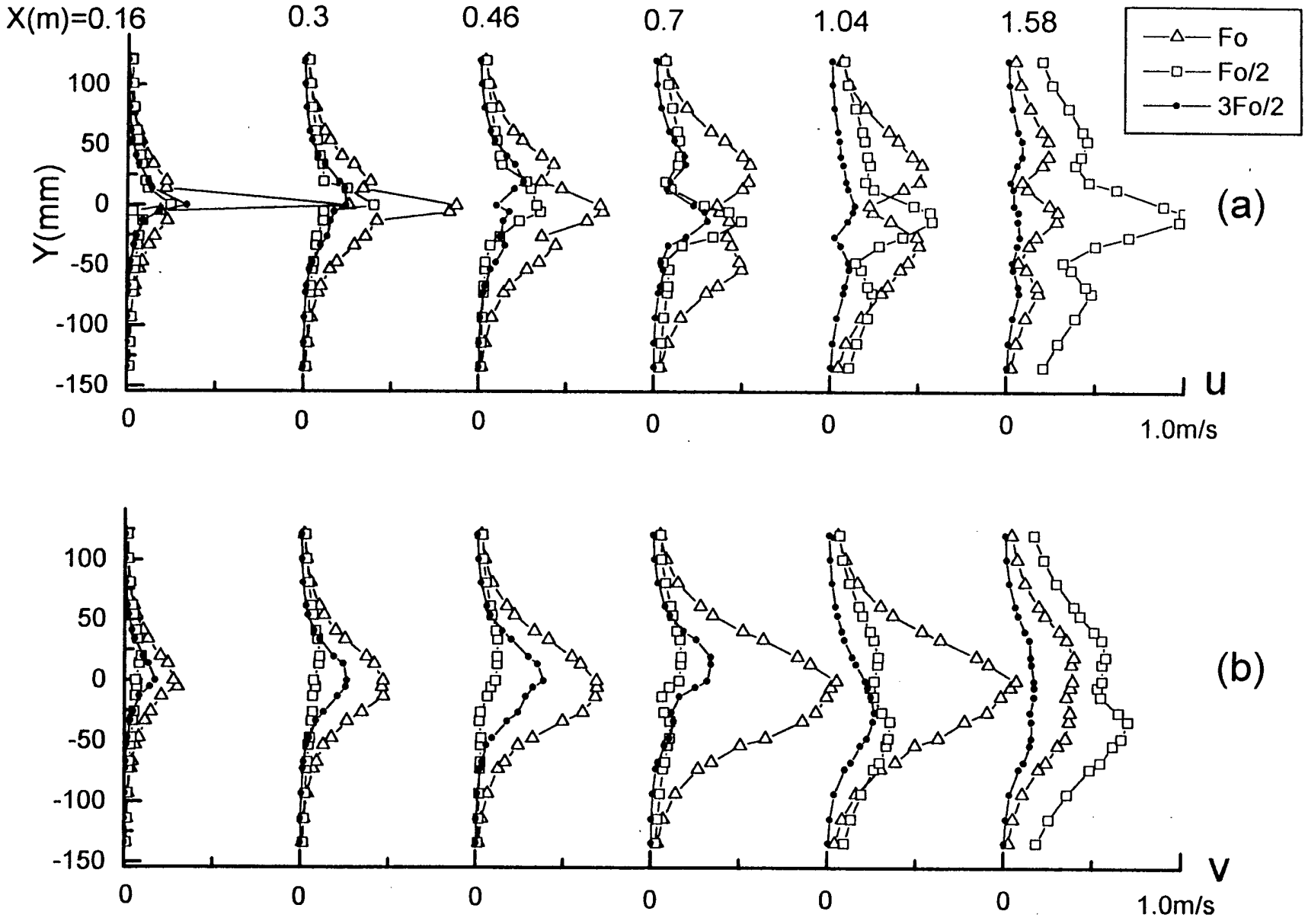

Fig.5.2 Amplitude distribution of the leading frequencies (TFW)

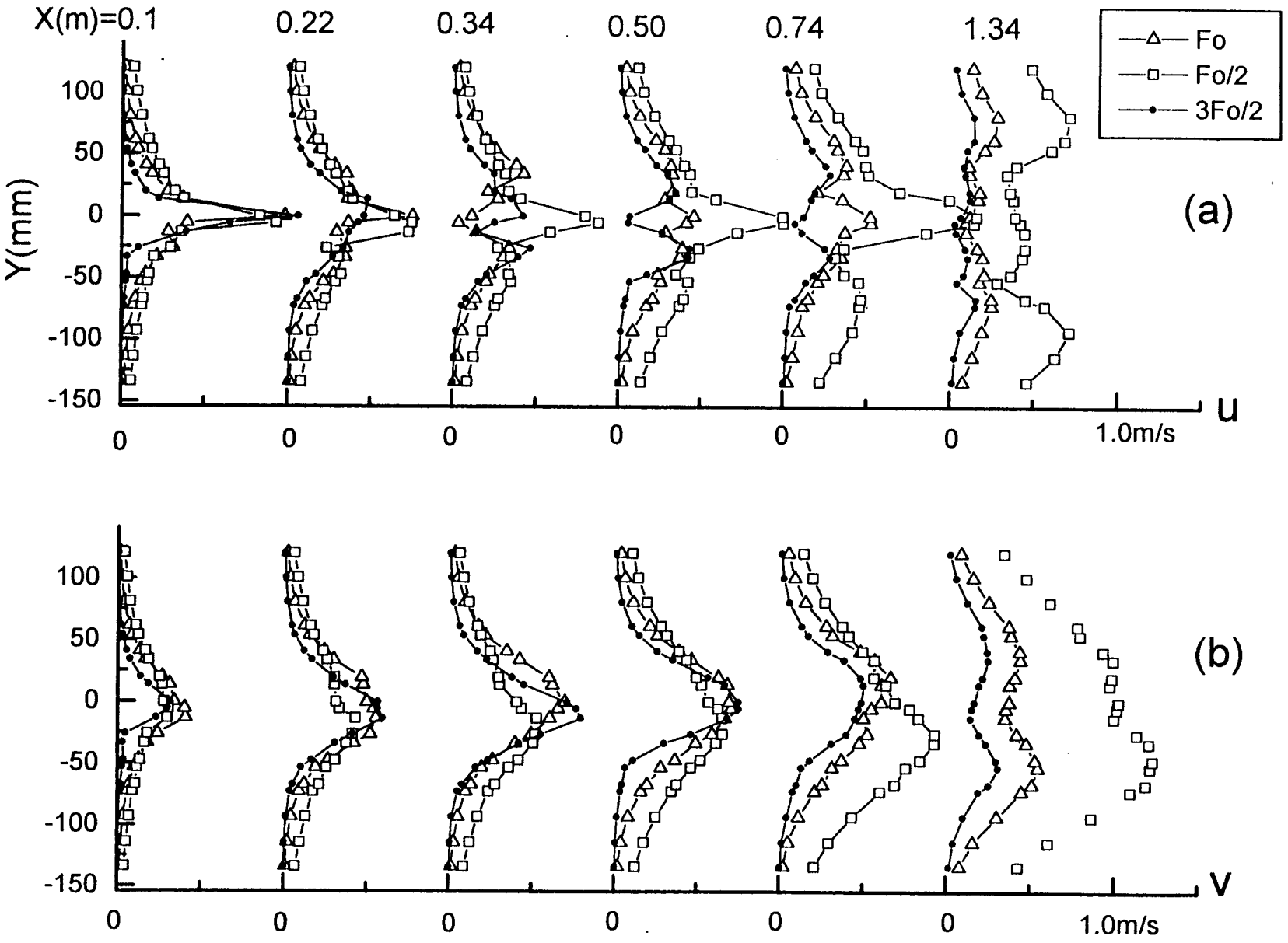

Fig.5.3 Amplitude distribution of the leading frequencies (TFS)

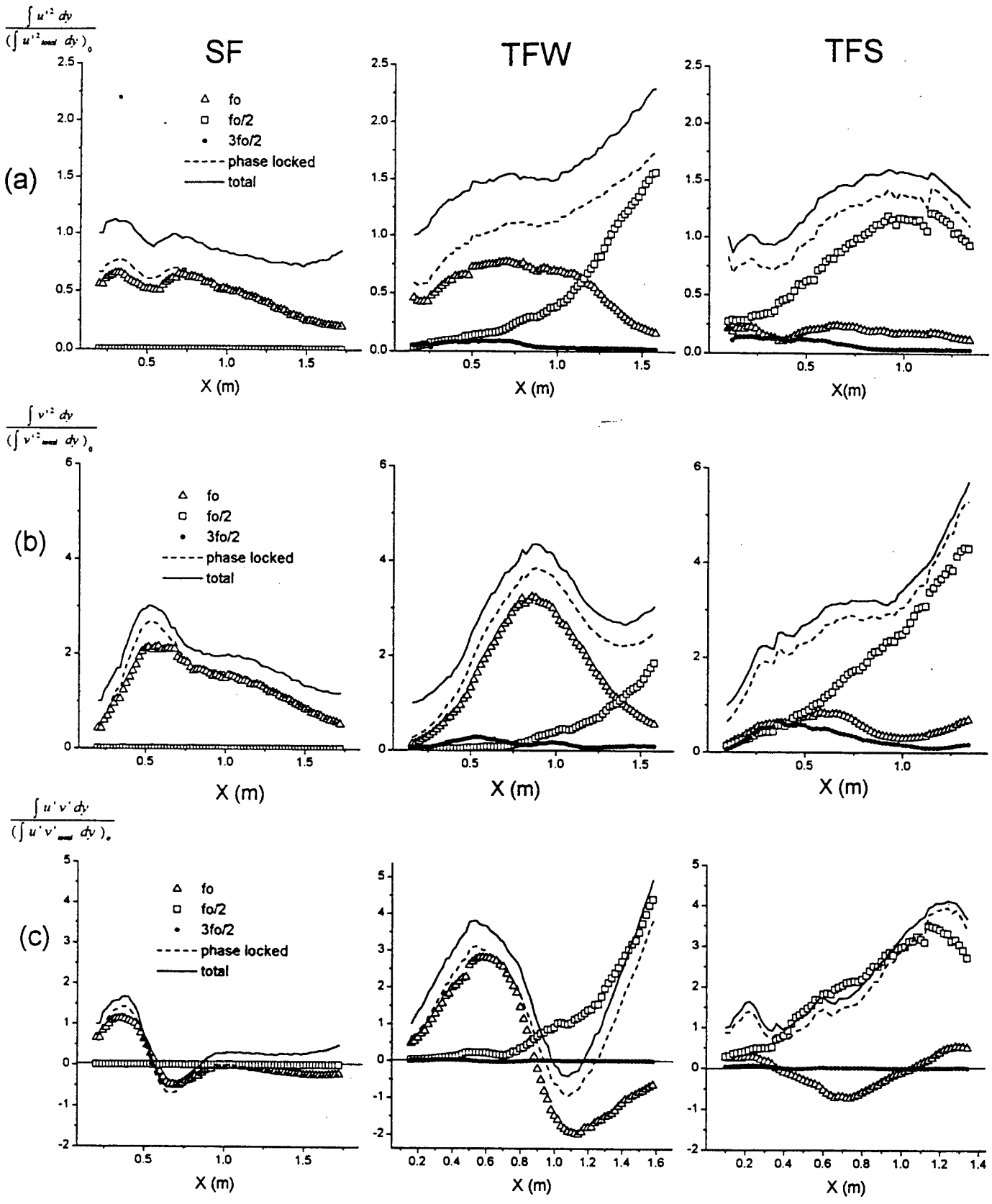

Fig.5.4 Streamwise development of coherent quantities

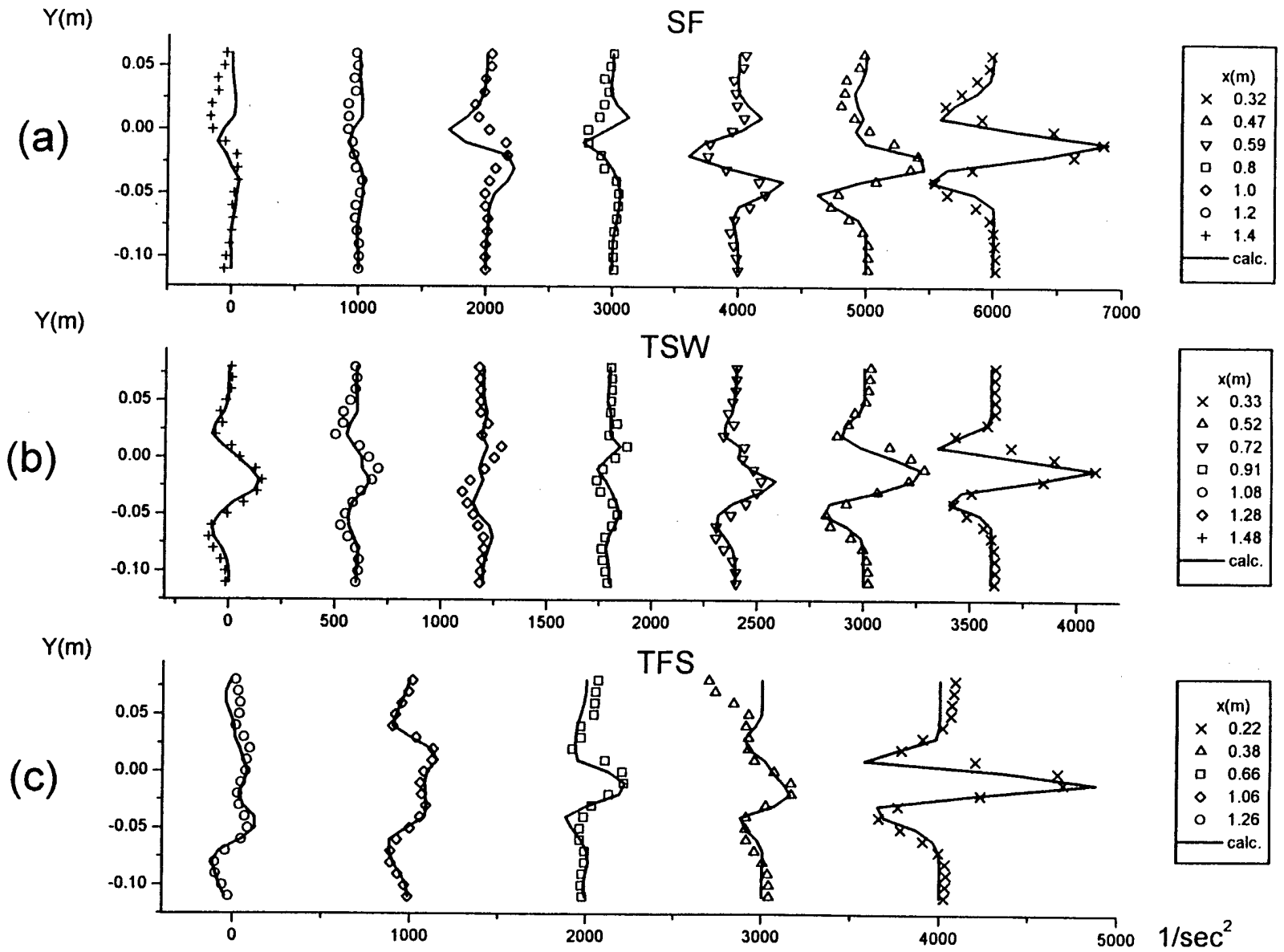

symbols --- measured rate of change of the mean vorticity (left side of the equation)
lines --- calculated rate of change from the right side of the equation

Fig.6.1 Mean vorticity balance

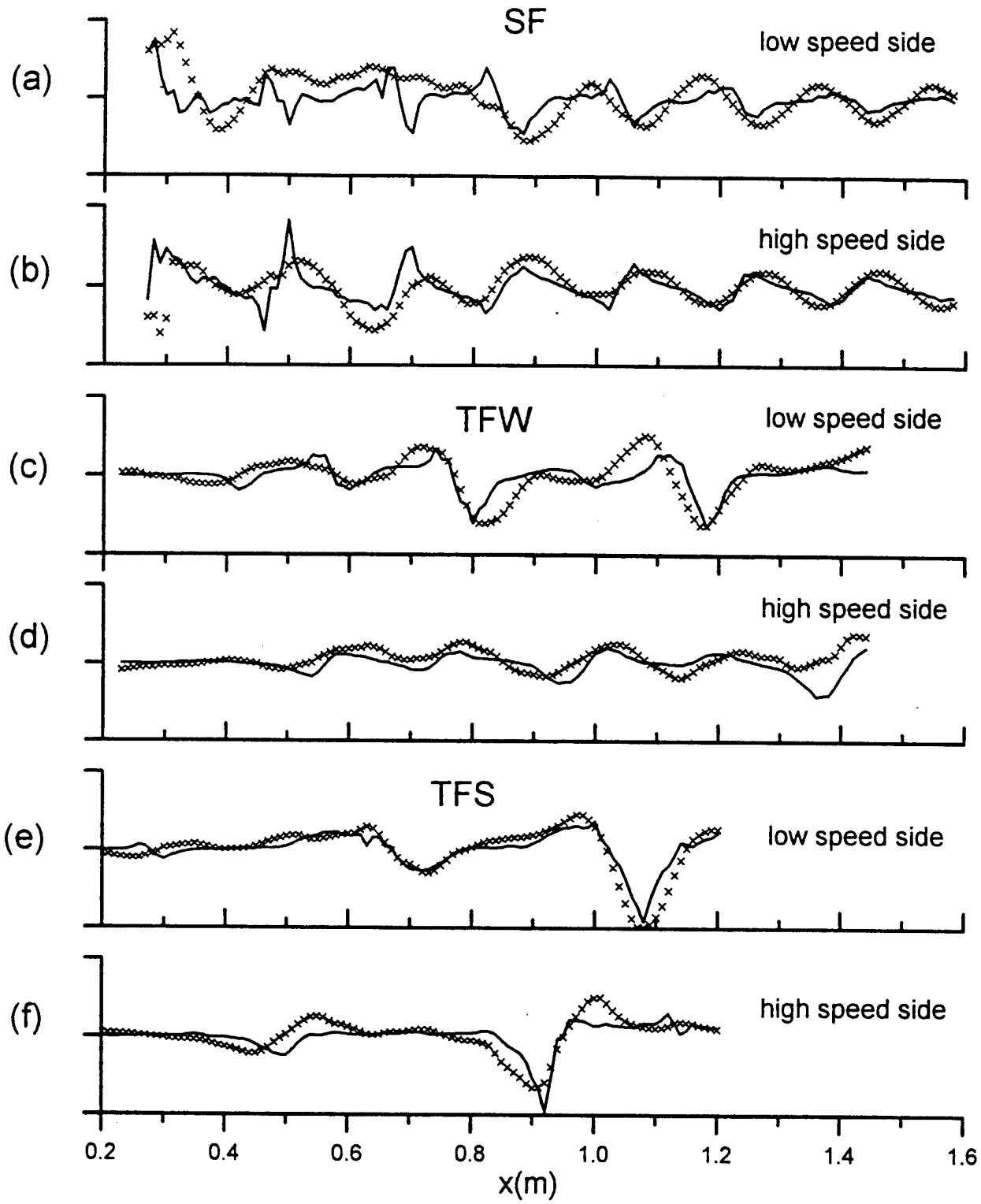

symbols --- measured rate of change of the coherent vorticity (left side of the equation)
lines --- calculated rate of change from the right side of the equation

Fig.6.2 Coherent vorticity balance

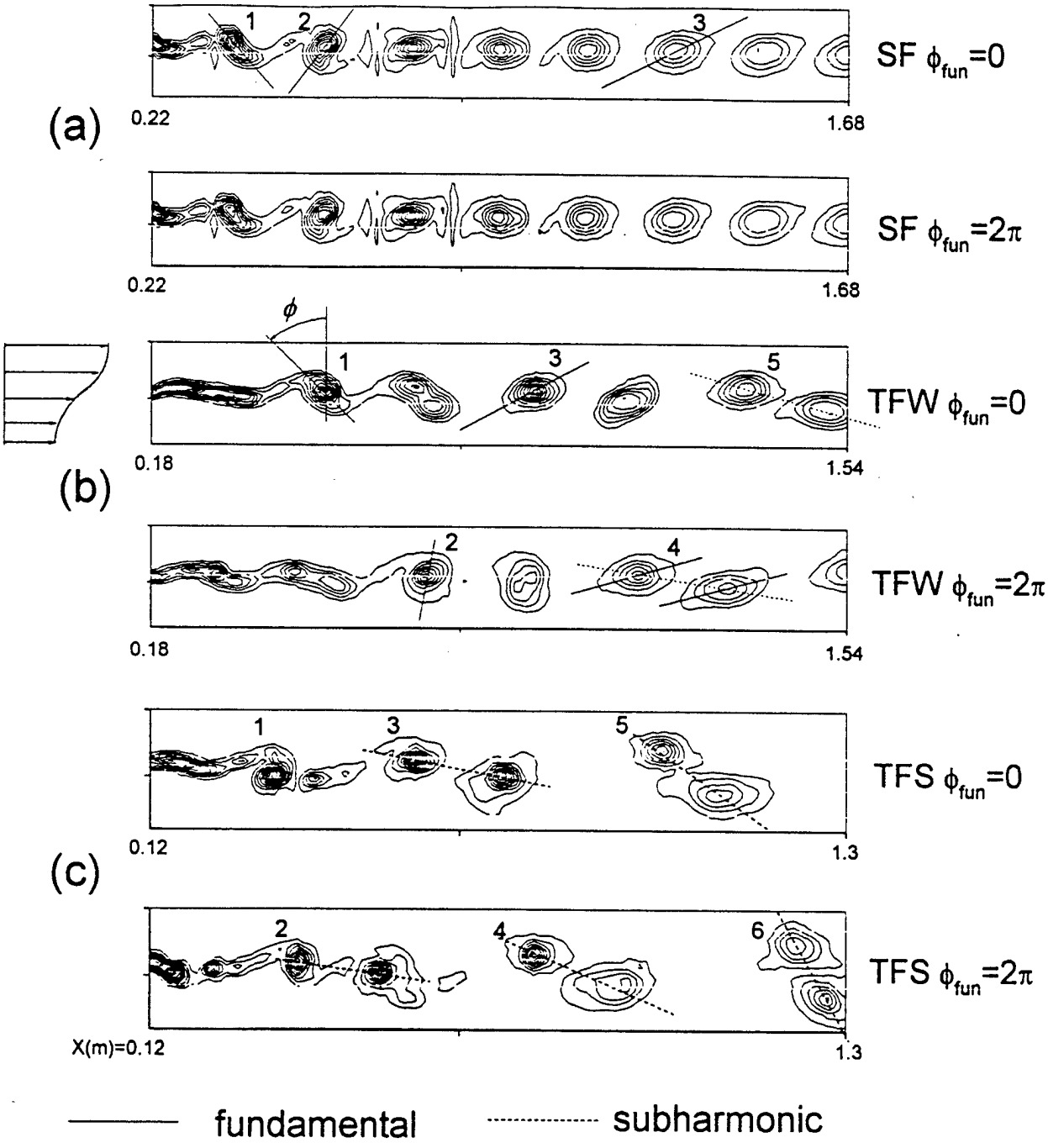

Fig.7.1 Vorticity contours of the forced mixing layer

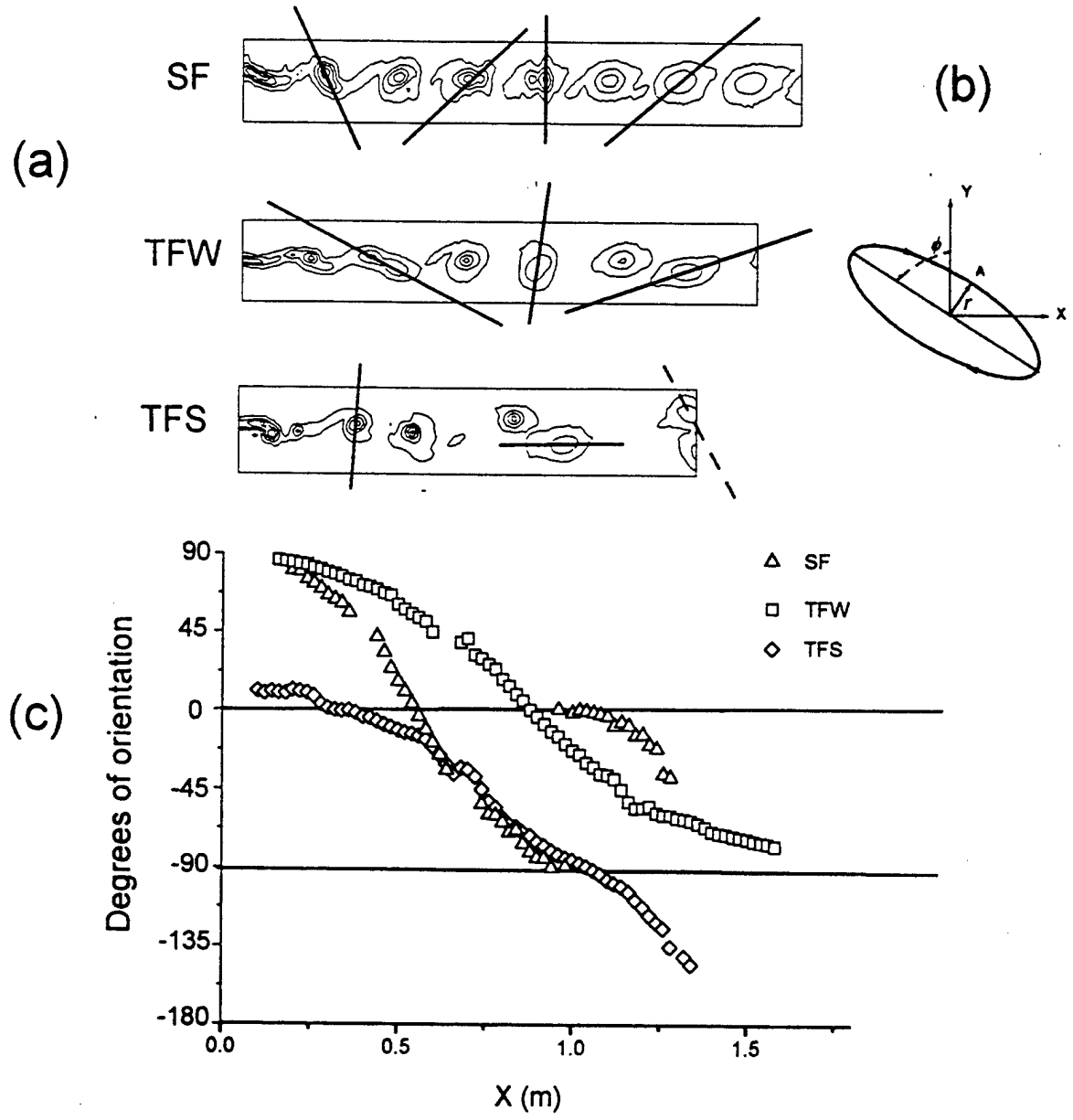

Fig.7.2 Calculated orientation of spanwise coherent vortices

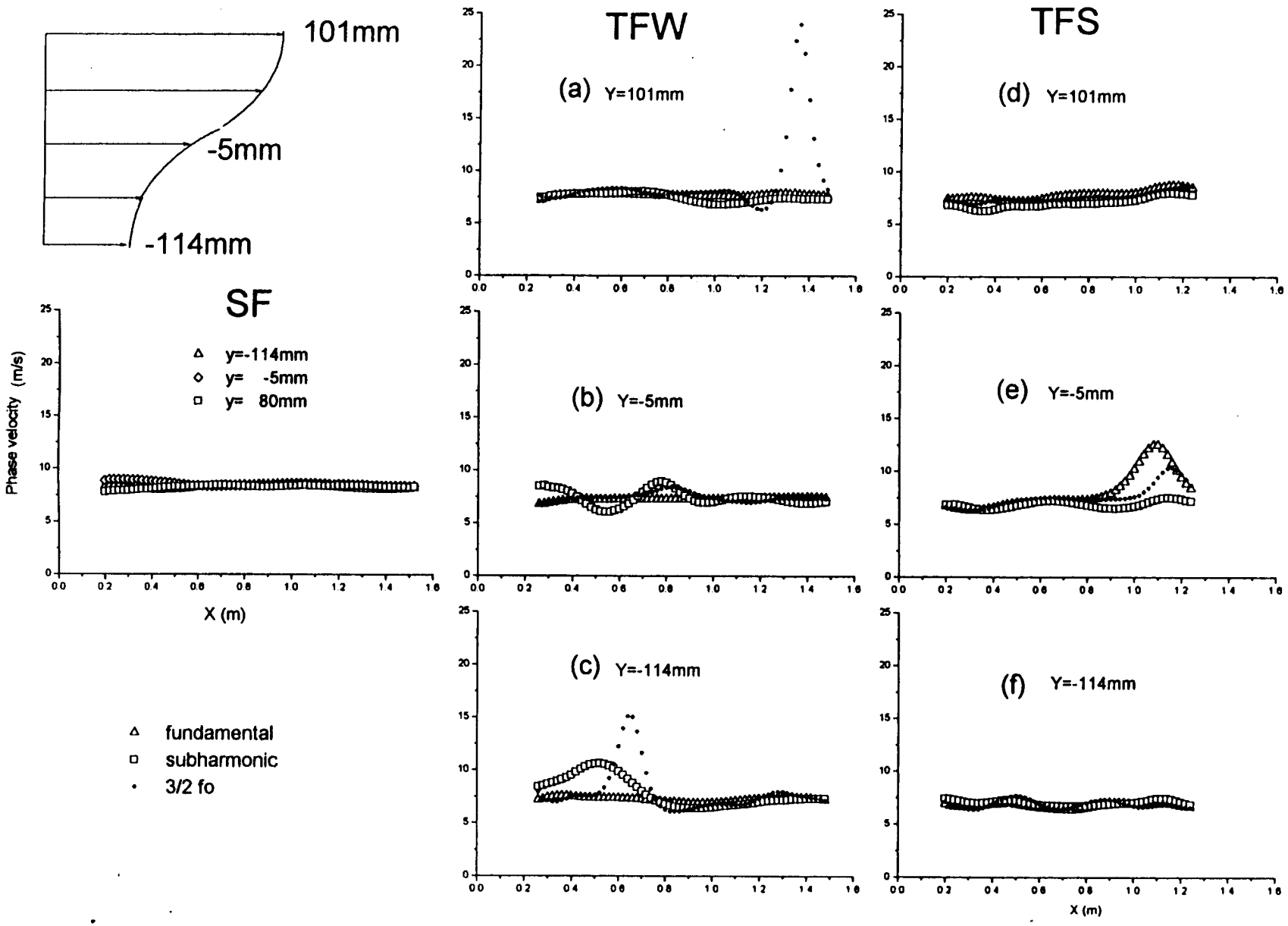

Fig.8.1 Streamwise phase velocity distribution of the coherent waves

$$\theta \frac{d}{dx} \log\{ \frac{\int_{-\infty}^{\infty} (u_c'^2 + v_c'^2) dy}{\int_{-\infty}^{\infty} (u_c'^2 + v_c'^2)_o dy} \}$$

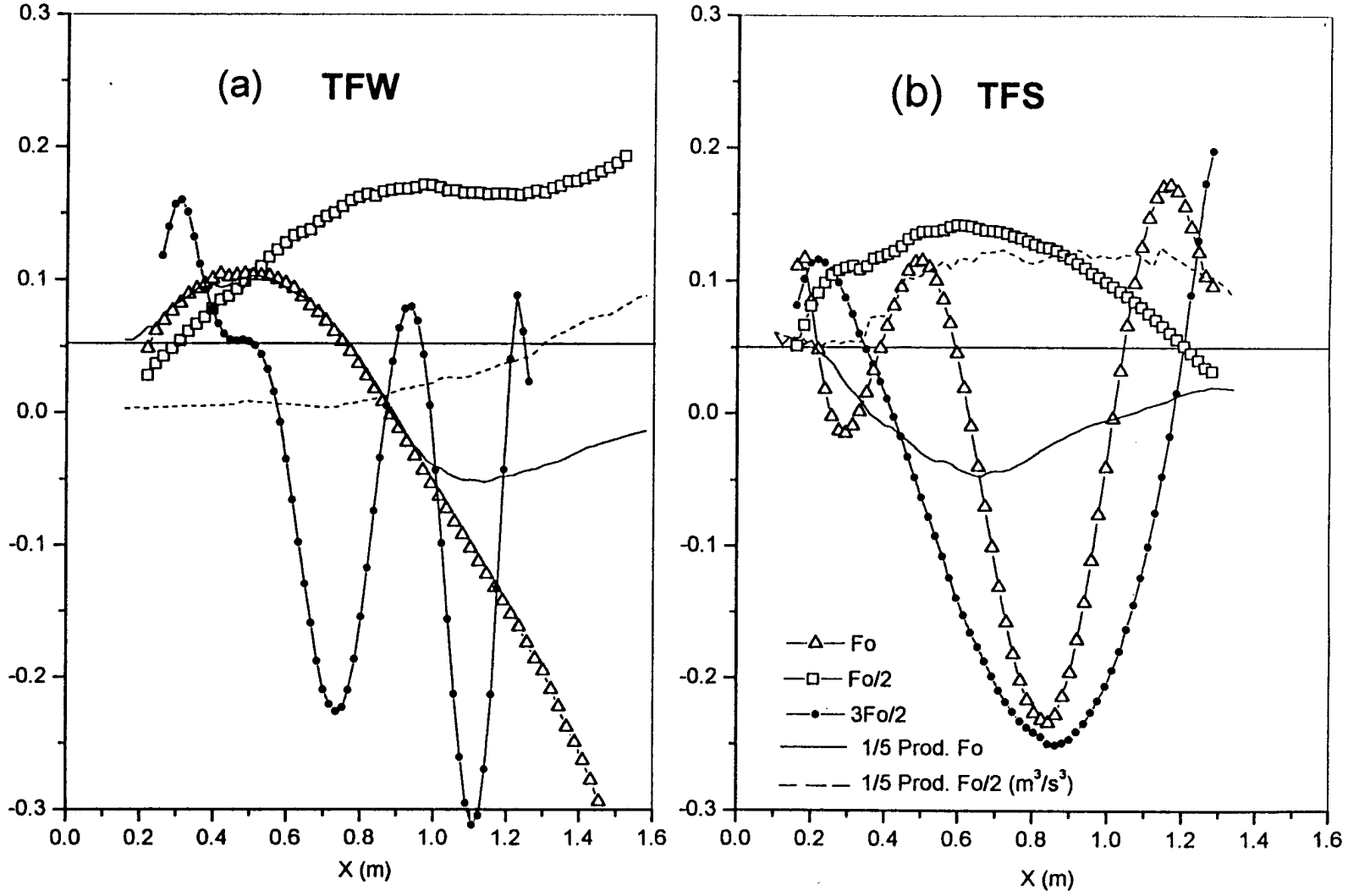

Fig.8.2 The amplification rate of coherent energy

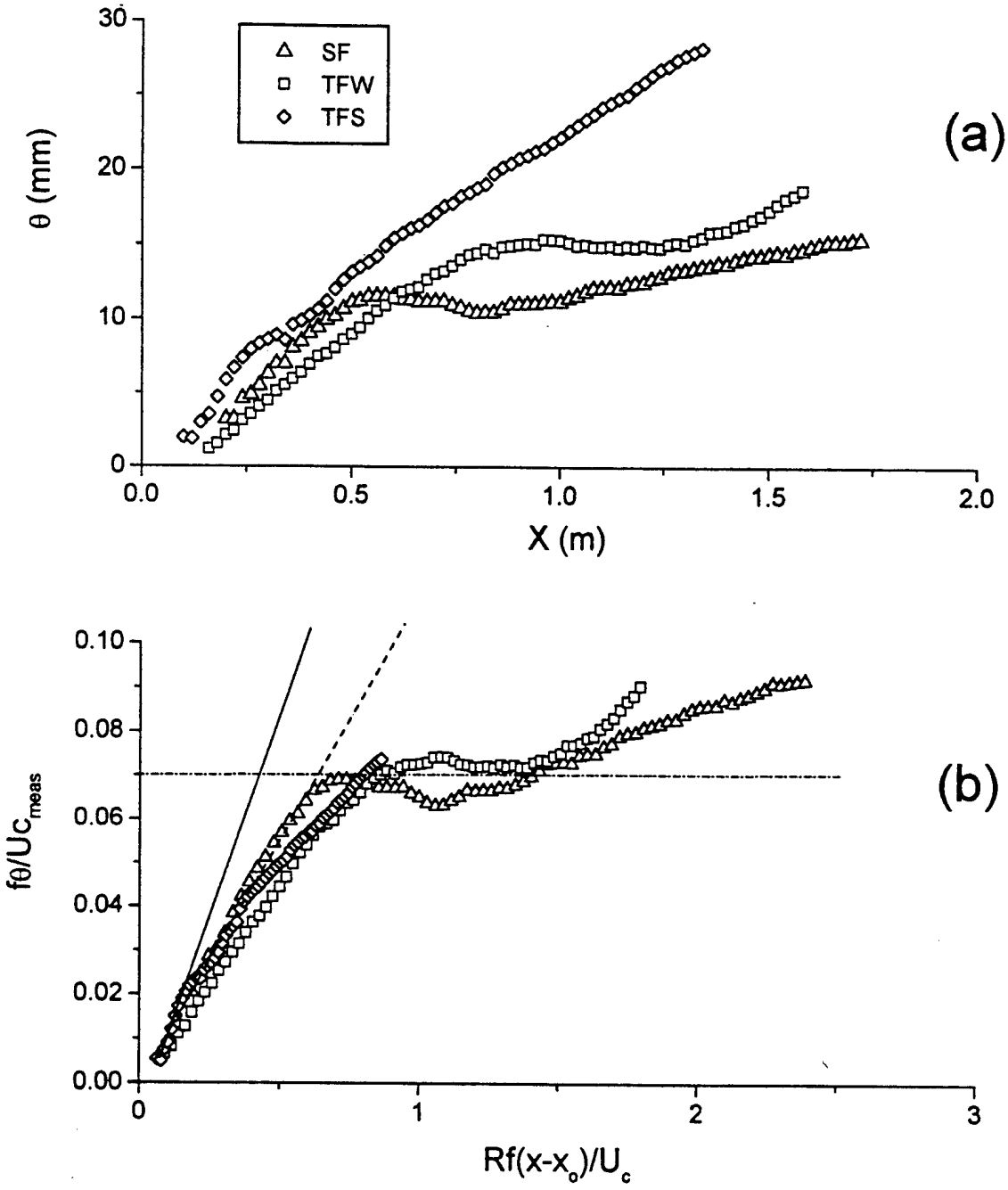

Fig.9.1 Streamwise distribution of the momentum thickness

(a) in physical dimensions

(b) normalized by dominant frequency and measured phase velocity